SOCIETY FOR EXPERIMENTAL BIOLOGY

Journal of Experimental Botany
https://doi.org/10.1093/jxb/eraf092 Advance Access Publication 23 March 2025

RESEARCH PAPER

Phenylacetic acid metabolism in land plants: novel pathways and metabolites

Pavel Hladík[1,2], Federica Brunoni[1,2], Asta Žukauskaitė[3], Marek Zatloukal[3], Jakub Bělíček[4], David Kopečný[4], Pierre Briozzo[5], Nathan Ferchaud[5], Ondřej Novák[1,2], and Aleš Pěnčík[1,2,*]

[1] Laboratory of Growth Regulators, Faculty of Science, Palacký University, Olomouc, Czech Republic
[2] Laboratory of Growth Regulators, Institute of Experimental Botany, The Czech Academy of Sciences, Olomouc, Czech Republic
[3] Department of Chemical Biology, Faculty of Science, Palacký University, Olomouc, Czech Republic
[4] Department of Experimental Biology, Faculty of Science, Palacký University, Olomouc, Czech Republic
[5] Université Paris-Saclay, INRAE, AgroParisTech, Institute Jean-Pierre Bourgin for Plant Sciences (IJPB), 78000, Versailles, France

* Correspondence: ales.pencik@upol.cz

Received 22 November 2024; Editorial decision 25 February 2025; Accepted 20 March 2025

Editor: Richard Napier, University of Warwick, UK

Abstract

In recent years, substantial progress has been made in exploring auxin conjugation and metabolism, primarily aiming at indole-3-acetic acid (IAA). However, the metabolic regulation of another key auxin, phenylacetic acid (PAA), remains largely uncharacterized. Here, we provide a comprehensive exploration of PAA metabolism in land plants. Through LC-MS screening across multiple plant species and their organs, we identified four previously unreported endogenous PAA metabolites: phenylacetyl-leucine, phenylacetyl-phenylalanine, phenylacetyl-valine, and phenylacetyl-glucose. Enzyme assays, genetic evidence, crystal structures, and docking studies demonstrate that PAA and IAA share core metabolic machinery, revealing a complex regulatory network that maintains auxin homeostasis. Furthermore, our study of PAA conjugation with amino acids and glucose suggests limited compensatory mechanisms within known conjugation pathways, pointing to the existence of alternative metabolic routes in land plants. These insights advance our knowledge of auxin-specific metabolic networks and highlight the unique complexity within plant hormone regulation.

Keywords: Auxin, conjugation, glucosyl ester, Gretchen Hagen 3, HPLC-MS/MS, indole-3-acetic acid, metabolism, phenylacetic acid, plant.

Introduction

Auxins are a class of phytohormones that are essential for coordinating plant growth and development. Indole-3-acetic acid (IAA) has been extensively investigated due to its diverse physiological impacts (Davies, 2010). Phenylacetic acid (PAA), another constituent of the auxin family, has recently gained attention due to its potential significance in plant

Abbreviations: GH3, GRETCHEN HAGEN 3; IAA, indole-3-acetic acid; IAA-AAs, indole-3-acetyl-amino acids; IAA-Asp, indole-3-acetyl-aspartate; IAA-glc, indole-3-acetyl-1-*O*-β-D-glucose; IAA-Glu, indole-3-acetyl-glutamate; IAR3, IAA-ALANINE RESISTANT 3; ILLs, ILR1-LIKE proteins; ILR1, IAA-LEUCINE RESISTANT 1; KKI, kakeimide; MST, microscale thermophoresis; oxIAA-AAs, 2-oxindole-3-acetyl-amino acids; oxIAA-glc, 2-oxindole-3-acetyl-1-*O*-β-D-glucose; PAA, phenylacetic acid; PAA-AAs, phenylacetyl-amino acids; PAA-Asp, phenylacetyl-aspartate;PAA-glc, phenylacetyl-1-*O*-β-D-glucose; PAA-Glu, phenylacetyl-glutamate; PAAld, phenylacetaldehyde; PAA-Leu, phenylacetyl-leucine; PAA-NHS, phenylacetic acid *N*-hydroxysuccinimide ester; PAA-Phe, phenylacetyl-phenylalanine; PAA-Trp, phenylacetyl-tryptophan; PAA-Val, phenylacetyl-valine;UGT,UDP-glycosyltransferase.

physiology and auxin signalling pathways. Although PAA accumulates more than IAA in most plant species, its homeostasis and function are not yet fully understood (Wightman and Lighty, 1982; Sugawara *et al.*, 2015; Cook, 2019). The auxin activity of PAA has been estimated to be less than 10% of that of IAA by three typical auxin tests: the cylinder test, the oat bending test, and the pea test (Haagen-Smit and Went, 1935). However, its main activity appears to be in lateral root induction and root growth promotion (reviewed in Cook, 2019; Perez *et al.*, 2023). Additionally, PAA has antimicrobial properties, exhibiting anti-fungal and anti-bacterial activities (Kawazu *et al.*, 1996; Liu *et al.*, 2014; Zhang *et al.*, 2022). Plants increase PAA production when attacked by herbivores, and exogenous PAA application has been reported to protect plants against fungal pathogens (Perez *et al.*, 2023). However, the exact biological function of PAA in plant defence mechanisms is still unclear and requires further evidence (Kunkel and Harper, 2018).

Biosynthesis of PAA originates from phenylalanine (Phe) and parallels IAA biosynthesis, albeit with different enzymes. Arogenate dehydratase alters PAA levels in Arabidopsis by converting arogenate to Phe, highlighting a Phe-dependent pathway (Aoi *et al.*, 2020b). The primary route involves converting Phe to phenylpyruvate, which then decarboxylates to PAA, similar to the IAA pathway (Cook *et al.*, 2016). However, enzymes responsible for this conversion, like phenylpyruvate aminotransferase from petunia, are still being studied (Yoo *et al.*, 2013; Cook *et al.*, 2016). Secondary pathways include converting Phe to phenylacetaldehyde (PAAld) via phenylacetaldehyde synthase (Kaminaga *et al.*, 2006) or to phenylethylamine by aromatic amino acid decarboxylases (Tieman *et al.*, 2006). Aldehyde dehydrogenase family 2 might be involved in the oxidation of PAAld to PAA as four maize isoforms were shown to be highly active towards many aromatic aldehydes including PAAld (Končitíková *et al.*, 2015). Additionally, a minor, stress-activated pathway converts Phe to phenylacetaldoxime via CYP79A2, which is directly converted to PAA in maize (Perez *et al.*, 2021).

The mechanisms for PAA inactivation employ similar pathways to those involved in IAA inactivation. The majority of the IAA in plants exists in its non-active form, which can be categorized into two main groups. The first comprises reversible storage forms, such as esters and amides, or methylated IAA. The second group consists of oxidized metabolites, which undergo irreversible metabolism leading to their degradation (reviewed in Casanova-Sáez *et al.*, 2021; Cohen and Strader, 2024). In PAA metabolism, only the first group has been described, as no oxidative metabolites had been identified. Earlier work in 2005 revealed that GRETCHEN HAGEN 3 (GH3) proteins, known for their role in forming IAA-amides with amino acids (IAA-AAs), also exhibit *in vitro* sensitivity to PAA (Staswick *et al.*, 2005). Subsequently, the first two conjugates, PAA-aspartate (PAA-Asp) and PAA-glutamate (PAA-Glu), were identified in transgenic Arabidopsis plants expressing β-estradiol-inducible YUCCA enzymes, whose induction led to the increase of endogenous levels of PAA-Glu by 14- to 41-fold and PAA-Asp levels by 1.6- to 3.8-fold (Sugawara *et al.*, 2015). The involvement of GH3 enzyme in PAA metabolism *in planta* has been confirmed in several studies. According to Sugawara *et al.* (2015), induction of *GH3.9* in β-estradiol-inducible Arabidopsis *GH3.9* transgenic plants resulted in an endogenous PAA-Glu level increase of 13-fold. Arabidopsis *GH3.5* overexpressing plants accumulated 15- to 70-fold higher PAA-Asp levels than wild-type plants, while PAA levels decreased by up to 5-fold (Westfall *et al.*, 2016). Moreover, the application of PAA or IAA to wild-type plants reciprocally reduced levels of opposite active auxin by increasing the corresponding aspartate metabolites in a GH3-dependent manner (Aoi *et al.*, 2020c). Other IAA metabolites conjugated with amino acids, such as IAA-Ala, -Gly, -Leu, -Phe, -Trp, and -Val, have also been detected in plants (Kowalczyk and Sandberg, 2001; Pěnčík *et al.*, 2009; Staswick, 2009). However, their concentrations are typically much lower than those of IAA-Asp and IAA-Glu, likely due to rapid conversion to free IAA mediated by enzymes such as IAA-LEUCINE RESISTANT 1 (ILR1), ILR1-LIKE proteins (ILLs), and IAA-ALANINE RESISTANT 3 protein (IAR3) (Bartel and Fink, 1995; Davies *et al.*, 1999; LeClere *et al.*, 2002), or through their oxidation to oxIAA-amino acids (oxIAA-AAs) (Hladík *et al.*, 2023). Notably, from these low-abundance amino acid conjugates, only PAA-Trp was identified in Arabidopsis at concentrations 17-fold higher than its IAA counterpart, suggesting a potential endogenous role for this PAA metabolite (Staswick *et al.*, 2017).

An alternative pathway in auxin metabolism involves the formation of glucosides, such as IAA or oxIAA glucosyl ester (IAA/oxIAA-glc), catalysed by the enzymes UDP- glycosyltransferases (UGT) 74D1 and UGT84B1 (Jackson *et al.*, 2001; Mateo-Bonmatí *et al.*, 2021). In *in vitro* experiments, both IAA and PAA have been shown to serve as substrates for UGT84B1. However, only IAA-glc has been detected *in vivo* (Grubb *et al.*, 2004; Aoi *et al.*, 2020a). IAA methylation, mediated by the IAA CARBOXYMETHYLTRANSFERASE 1 (IAMT1) enzyme, has been demonstrated in plants (Qin *et al.*, 2005). However, overexpression of IAMT1 in Arabidopsis did not lead to a reduction in PAA levels, suggesting that this enzyme is not responsible for PAA methylation in plants. Nevertheless, PAA methyl ester has been identified in *Escherichia coli* and therefore its presence in plants cannot be ruled out (Takubo *et al.*, 2020). Regardless of whether PAA has been widely detected in the plant kingdom, mechanisms for its inactivation, which may be shared among other species, have only been investigated in Arabidopsis.

Despite recent discoveries in PAA homeostasis, our understanding of how PAA is metabolized in plants remains incomplete. In this study, we identified PAA glucosyl ester (PAA-glc) *in planta* for the first time, as well as three novel endogenous amino acid conjugates, phenylacetyl-leucine

(PAA-Leu), phenylacetyl-phenylalanine (PAA-Phe) and phenylacetyl-valine (PAA-Val). Quantitative profiling of a range of PAA metabolites across a spectrum of model plant species, spanning from bryophytes to angiosperms, performed by high-performance liquid chromatography–tandem mass spectrometry (HPLC-MS/MS), revealed differences in PAA metabolism as distribution of conjugates differed notably among the studied species as well as their organs. To elucidate PAA metabolic pathways, we further performed bacterial enzyme assays to identify the candidate enzymes for inactivation/activation of PAA and expanded those finding *in planta* by a feeding assay using PAA in different genetic backgrounds or upon chemical knockdown of the IAA-conjugation pathway.

Materials and methods

Reagents and standards

Plant agar and Murashige and Skoog (MS) medium were purchased from Duchefa (Haarlem, Netherlands). Hypergrade purity methanol for HPLC-MS/MS analysis and all other chemicals were purchased from Lach-Ner (Neratovice, Czech Republic), Merck KGaA (Darmstadt, Germany), and Sigma-Aldrich (St Louis, MO, USA). Standards for PAA and $^{13}C_6$-labeled PAA were purchased from Merck KGaA (Darmstadt, Germany). IAA-glc and [$^{13}C_6$]IAA-glc were synthesized according to Kai et al. (2007a, b) with minor modifications. Selected L-amino acid (Val, Leu, Phe, Trp, Asp, Glu) conjugates with PAA, including isotopically labelled standards [$^{13}C_6$]PAA-Asp and [$^{13}C_6$]PAA-Glu, were prepared according to Illić *et al.* (1997). PAA-glc was synthesized adopting reaction conditions from Takeuchi *et al.* (2020).

Synthesis of phenylacetic acid conjugates

Chemicals and general methods

Chemicals and solvents were purchased from common commercial suppliers. All reactions were performed in oven-dried glassware. Conversion of starting materials was monitored by thin layer chromatography on aluminium plates coated with silica gel 60 F254 (Merck, USA) and the reaction components were visualized by UV light (254 and 365 nm) and staining solutions (ninhydrin or potassium permanganate). Reaction mixtures were purified by crystallization or column chromatography on silica gel (40–63 µm Davisil LC60A, Grace Davison, UK). ^{1}H (500 MHz) and ^{13}C (125 MHz) NMR spectra were recorded in deuterated solvents at room temperature on a Jeol ECA-500 spectrometer equipped with a 5 mm Royal probe and compared with reported data. The LC-MS analyses were performed on an ACQUITY UPLC H-Class system combined with UPLC PDA detector and a single-quadrupole mass spectrometer QDa (Waters, UK) as described previously (Bieleszová *et al.*, 2019).

Synthesis of phenylacetic acid N-hydroxysuccinimide ester and $^{13}C_6$-phenylacetic acid N-hydroxysuccinimide ester

Phenylacetic acid (1950 mg, 14.3 mmol) was dissolved in dioxane/ethyl acetate (15/7; 22 ml), cooled down to 0 °C and *N*-hydroxysuccinimide (1730 mg, 15 mmol) and *N*,*N*′-dicyclohexylcarbodiimide (3090 mg, 15 mmol) were added sequentially. The reaction mixture was brought up to room temperature and stirred for 1 h. Upon completion, the reaction mixture was cooled down to 0 °C, fileted through a pad of Celite, and the filter cake was washed with dioxane–ethyl acetate (3:1, 2×15 ml). The filtrate was evaporated to dryness and the residue was purified by crystallization from 2-propanol (30 ml) to give pure phenylacetic acid *N*-hydroxysuccinimide ester (PAA-NHS; 3.010 g, 90%), the spectral data of which were in good agreement with the published data (Zasedateleva *et al.*, 2020). [$^{13}C_6$]PAA-NHS was prepared analogously using [$^{13}C_6$]PAA as a starting material.

Synthesis of phenylacetyl-aspartate and $^{13}C_6$-phenylacetyl-aspartate

PAA-NHS (1000 mg, 4.25mmol) was reacted with L-aspartic acid sodium salt (769 mg, 4.96 mmol) in dioxane–water (1:1, 80 ml) at room temperature for 3 h. Upon completion, the reaction mixture was cooled down to 0 °C, acidified with 1 M HCl to pH 2.5–3 and extracted with ethyl acetate (3×40 ml). Combined organic extracts were washed with brine (40 ml), dried over sodium sulphate, and evaporated to dryness. The residue was purified by column chromatography to give pure PAA-Asp (570 mg, 53%), the spectral data of which were in good agreement with the published data (Thangavelu *et al.*, 2017). [$^{13}C_6$]PAA-Asp was prepared analogously using [$^{13}C_6$]PAA-NHS as a starting material.

Synthesis of phenylacetyl-glutamate and $^{13}C_6$-phenylacetyl-glutamate

PAA-NHS (500 mg, 2.14 mmol) was reacted with L-glutamic acid sodium salt (419 mg, 2.48 mmol) in dioxane–water (1:1, 40 ml) at room temperature for 3 h. Upon completion, the reaction mixture was cooled down to 0 °C, acidified with 1 M HCl to pH 2.5–3 and extracted with ethyl acetate (3×20 ml). Combined organic extracts were washed with brine (20 ml), dried over sodium sulphate, and evaporated to dryness. The residue was purified by column chromatography to give pure PAA-Glu (195 mg, 34%), the spectral data of which were in good agreement with the published data (Thangavelu *et al.*, 2017). [$^{13}C_6$]PAA-Glu was prepared analogously using [$^{13}C_6$]PAA-NHS as a starting material.

Synthesis of phenylacetyl-valine

PAA-NHS (1500 mg, 6.4 mmol) was reacted with L-valine sodium salt (1043 mg, 7.5 mmol) in dioxane–water (1:1, 100 ml) at room temperature for 3 h. Upon completion, reaction mixture was cooled down to 0 °C, acidified with 1 M HCl to pH 2.5–3 and extracted with ethyl acetate (3×50 ml). Combined organic extracts were washed with brine (50 ml), dried over sodium sulphate, and evaporated to dryness. The residue was purified by column chromatography to give pure PAA-Val (1400 mg, 92%), the spectral data of which were in good agreement with the published data (Schwieter and Johnston, 2016).

Synthesis of phenylacetyl-phenylalanine

PAA-NHS (1500 mg, 6.4 mmol) was reacted with L-phenylalanine sodium salt (1404 mg, 7.5 mmol) in dioxane–water (1:1, 100 ml) at room temperature for 3 h. Upon completion, the reaction mixture was cooled down to 0 °C, acidified with 1 M HCl to pH 2.5–3 and extracted with ethyl acetate (3×50 ml). Combined organic extracts were washed with brine (50 ml), dried over sodium sulphate and evaporated to dryness. The residue was purified by column chromatography to give pure PAA-Phe (1311 mg, 72%), the spectral data of which were in good agreement with the published data (Schwieter and Johnston, 2016).

Synthesis of phenylacetyl-leucine

PAA-NHS (1500 mg, 6.4 mmol) was reacted with L-leucine sodium salt (1149 mg, 7.5 mmol) in dioxane–water (1:1, 100 ml) at room temperature for 3 h. Upon completion, the reaction mixture was cooled down to 0 °C, acidified with 1 M HCl to pH 2.5–3 and extracted with ethyl acetate (3×50 ml). Combined organic extracts were washed with brine (50 ml), dried over sodium sulphate, and evaporated to dryness. The residue was purified by column chromatography to give pure PAA-Leu (1395 mg, 87%), the spectral data of which were in good agreement with the published data (Gabor and Janssen, 2004).

Synthesis of phenylacetyl-tryptophan

PAA-NHS (1500 mg, 6.4 mmol) was reacted with L-tryptophan sodium salt (1697 mg, 7.5 mmol) in dioxane–water (1:1, 100 ml) at room temperature for 3 h. Upon completion, reaction mixture was cooled down to 0 °C, acidified with 1 M HCl to pH 2.5–3 and extracted with ethyl acetate (3×50 ml). Combined organic extracts were washed with brine (50 ml), dried over sodium sulphate, and evaporated to dryness. The residue was purified by column chromatography to give pure PAA-Trp (1120 mg, 54%), the spectral data of which were in good agreement with the published data (Matsui *et al.*, 2021).

Synthesis of phenylacetyl-glucose

Glucose (199 mg, 1.1 mmol) was was dissolved in anhydrous dioxane (37 ml) and sonicated under argon for 15 min. Subsequently, PAA (50 mg, 0.37 mmol) and triphenylphosphine (193 mg, 0.74 mmol) were added to the reaction mixture, followed by dropwise addition of diisopropyl azodicarboxylate (144 µl, 0.74 mmol). The resulting mixture was stirred vigorously at room temperature for 30 min, quenched with methanol, and evaporated to dryness. The residue was purified by column chromatography to give pure PAA-glc (52 mg, 47%), the spectral data of which were in good agreement with the published data (Iddon *et al.*, 2011).

Plant material and growth conditions

Arabidopsis seeds of ecotype Columbia 0 (Col-0) were used as wild type for all the experiments. Knockout mutant lines *gh3.1*, *2*, *3*, *4*, *5*, *6* (*gh3sex*) (Porco *et al.*, 2016), *ugt74d1*, and *ugt84b1* (Mateo-Bonmatí *et al.*, 2021) were obtained from Prof. Karin Ljung (Umeå Plant Science Centre, Sweden). Arabidopsis, maize (*Zea mays* L.), pea (*Pisum sativum arvense* L.), and wheat (*Triticum aestivum* L.) were cultivated as previously published in Hladík *et al.* (2023). Gametophores from *Physcomitrium patens* and spruce (*Picea abies* L. Karst) plants were cultivated as described in Brunoni *et al.* (2023). All the plants were harvested [~10 mg fresh weight (FW)] at growth stage 1.0 according to the Biologische Bundesanstalt, Bundessortenamt und Chemische Industrie (BBCH) scale (Tottman, 1987; Lancashire *et al.*, 1991; Boyes *et al.*, 2001) (except *P. patens*, which was harvested 3 weeks after the last gametophores transfer to fresh medium).

Feeding experiments

For PAA treatments, 7 days after germination (DAG), Arabidopsis seedlings (Col-0 and *gh3sex*) grown under the same conditions as described above were harvested, washed in ultrapure water, and transferred to liquid medium (half-strength MS medium, 1% sucrose, pH 5.7) supplemented with 20 µM PAA. Plants were shaken gently in the dark at 22 °C and harvested after 0.5, 1, and 3 h. For kakeimide (KKI) (Fukui *et al.*, 2022) treatments, 7 DAG Arabidopsis seedlings, 14 DAG spruce plants, and 3-week-old *P. patens* gametophores were transferred to sterile liquid Knop medium for 1, 6, and 24 h, depending on the species, according to Fukui *et al.* (2022) and Brunoni *et al.* (2023) and then supplemented with 5 µM PAA, 50 µM KKI, or a combination of 5 µM PAA with 50 µM KKI. Mock-treated Arabidopsis, *P. patens* and spruce plants were used as controls. Plants were harvested in five biological replicates per time point (~10 mg FW), immediately snap-frozen in liquid nitrogen, and stored at −80 °C.

Cloning, protein production, and bacterial enzyme assay

Escherichia coli BL21 (DE3) strain expressing recombinant AtGH3s, AtUGTs, and AtILR1/ILLs used in this work were previously generated (Brunoni *et al.*, 2019; Široká *et al.*, 2025). Recombinant protein production and enzymatic assay of AtGH3s, AtUGTs, and AtILR1/ILLs were performed as described previously by Brunoni *et al.* (2019; 2023) and Široká *et al.* (2025). For the amino acid conjugation assay, 500 µl of clarified cell lysate from AtGH3.6- or AtGH3.17-producing bacterial cultures was incubated with GH3 cofactors with or without 0.1 mM PAA. For the glucose conjugation assay, 500 µl of clarified cell lysate from AtUGT84B1- or AtUGT74D1-producing bacterial cultures was incubated with UGT cofactors with or without 0.1 mM PAA/IAA. For the hydrolysis assay, 500 µl of clarified cell lysate from AtILL2-, AtILL6-, AtILR1-, or AtIAR3-producing bacterial cultures was incubated with 1 mM $MgCl_2$ with or without 0.1 mM PAA-Leu, PAA-Trp, PAA-Val, or PAA-Glu. Green fluorescent protein (GFP)-producing bacterial cultures were used as negative controls. The enzymatic activity of the recombinant proteins was tested for 5 h at 30 °C with constant shaking at 50 rpm in darkness and repeated in three biological replicates.

Phenylacetic acid conjugate profiling

Extraction and purification of PAA conjugates followed the methodology described by Hladík *et al.* (2023) with modifications. Samples containing ~10 mg fresh weight of tissue were extracted in 1 ml of an ice-cold sodium phosphate buffer (50 mM, pH 7.0) supplemented with 0.1% diethyldithiocarbamic acid sodium salt. A mixture of isotopically labelled internal standards was added to the samples, including [$^{13}C_6$]PAA (10 pmol), [$^{13}C_6$]PAA-Asp (5 pmol), and [$^{13}C_6$]PAA-Glu (5 pmol). The samples were homogenized using an MM400 bead mill (Retsch GmbH, Haan, Germany) with three zirconium oxide beads. The samples were then incubated on a rotary shaker (15 min, 27 rpm, 4 °C) and then centrifuged (10 min, 206 642 *g*, 4 °C). From the supernatant, 200 µl was acidified with 1 M HCl to pH 2.7 and subjected to purification by in-tip micro solid-phase extraction (in-tip µSPE) utilizing a combination of HLB AttractSPE (Affinisep, Le Houlme, France) and SDB-XC Empore (3M, St Paul, MN, USA) sorbents. The multi-StageTip microcolumns were activated sequentially with 50 µl of acetone (centrifugation for 10 min, 3846 *g*, 8 °C), 50 µl of methanol (10 min, 3846 *g*, 8 °C), and 50 µl of water (15 min, 4654 *g*, 8 °C). The acidified samples were then applied to the activated microcolumns (30 min, 16 961 *g*, 8 °C), washed with 50 µl of 0.1% acetic acid (20 min, 9846 *g*, 8 °C), and eluted with 50 µl of 80% methanol (20 min, 8653 *g*, 8 °C). After elution, samples were evaporated to dryness under vacuum and stored at −20 °C until HPLC-MS/MS analysis.

Evaporated samples were reconstituted in 30 µl of 10% methanol prior to analysis on an HPLC-MS/MS system consisting of a 1260 Infinity LC II system (Agilent Technologies, Santa Clara, CA, USA) equipped with a reversed-phase chromatographic column (Kinetex C18 100 Å, 50×2.1 mm, 1.7 µm; Phenomenex, Torrance, CA, USA) and coupled to a 6495B Triple Quadrupole LC/MS system (Agilent Technologies). The mobile phase consisted of deionized water (A) and methanol (B) supplemented with 0.1% acetic acid. The chromatographic analysis was carried out for 18 min at a flow rate of 0.3 ml min^{-1}. The elution of auxin metabolites was achieved using a gradient: 0 min, 10% B; 11.5 min, 60% B; 11.75 min, 99% B; 14.75 min, 99% B; 15 min, 10% B. During analysis, samples were stored in an autosampler at 4 °C, with the column maintained at 40 °C, and 10 µl of each sample was injected.

Individual analytes were detected using the MS instrument operating in negative electrospray ionization (ESI−) mode with optimized parameters: nebulizer pressure at 25 psi, drying gas flow rate and temperature set at 14 l min^{-1} and 130 °C, respectively, sheath gas flow rate and temperature set at 12 l min^{-1} and 400 °C, respectively, capillary voltage set at 3.0 kV, and nozzle voltage maintained at 0 V. The measured analytes were detected and quantified by diagnostic multiple reaction monitoring transitions of precursor and appropriate product ions using optimal collision energies and a dwell time of 50 ms, as described in Supplementary Table S1. Raw data analysis was performed using Mass Hunter software (Agilent Technologies).

For method validation, a 15 point calibration curve was prepared ranging from 9 amol to 90 pmol and the limit of detection (LOD) (S/N ratio >3) was calculated as well as the dynamic linear range (Supplementary Table S1). The validation protocol followed an approach published in Hladík *et al.* (2023). Arabidopsis and pea plants were harvested at growth stage 1.0 and spiked by 0, 1, and 10 pmol of authentic PAA standards (0, 10, and 50 pmol for PAA-glc), and 5 pmol of internal standards ([$^{13}C_6$]PAA, [$^{13}C_6$]PAA-Asp, [$^{13}C_6$]PAA-Glu). All samples were then extracted and purified as described above and measured by HPLC-MS/MS. After the measurement, analyte accuracy (percentage bias) and precision (relative standard deviation in %) was calculated (Supplementary Tables S2, S3).

Statistical analyses

All analyses were performed using R statistical software (version 4.3.2; R Core Team, 2021) within the RStudio environment (version 2023.12.0.369; Posit Team, 2023). The following packages were used for statistical analysis and graph generation: dplyr (Wickham *et al.*, 2023), ggplot2 (Wickham, 2016), ggbreak (Xu *et al.*, 2021), multcomp (Hothorn *et al.*, 2008), multcompview (Graves *et al.*, 2019), and readxl (Wickham and Bryan, 2023).

One-way ANOVA was used to assess differences between control and experimental variants. Significant differences detected at the 95% confidence level were subjected to Tukey's post-hoc test. Values under the LOD were replaced with 0.66-fold the respective LOD value. For data visualization, box-and-whisker plots were generated showing the median (centre line), upper and lower quartiles (box limits), and maximum and minimum values, with individual dots representing each biological replicate.

Expression and purification of AtGH3.6 protein

A protein expression construct harbouring the coding sequence of AtGH3.6 (TAIR accession no. AT5G54510) was previously generated (pETM11-AtGH3.6, Brunoni *et al.*, 2019), transformed into *E. coli* Rosetta (DE3) cells, and grown in Luria broth containing 50 μg ml^{-1} kanamycin and 20 μg ml^{-1} chloramphenicol to OD_{600}≈0.8. Protein expression was induced with 1 mM isopropyl-β-D-thiogalactopyranoside overnight at 20 °C. Cell lysis and protein extraction were performed as described in Brunoni *et al.* (2023). The recombinant protein was purified on a Nickel-HiTrap IMACFF column (Cytiva Life Sciences, Marlborough, MA, USA) on an NGC Medium-Pressure Liquid Chromatography System into 50 mM HEPES (pH 7.5) and 300 mM NaCl. The His-tagged protein was further purified by anion exchange chromatography on a Resource Q column (Cytiva Life Sciences). Equilibration buffer was 50 mM HEPES (pH 7.5)–1 mM $MgCl_2$. The elution buffer additionally contained 1 M NaCl. The purified protein was desalted by diafiltration using 50 kDa-cutoff Centricon filters (Millipore, Bedford, MA, USA). Protein concentration was determined by Bradford assay with BSA as the standard.

Crystallization of AtGH3.6 and structure determination

Crystallization conditions for AtGH3.6 were screened using a Qiagen PEGS II suite kit (Qiagen, Hilden, Germany). Crystals of AtGH3.6 were obtained in hanging drops by mixing equal volumes of (i) enzyme solution (7.1 mg ml^{-1} for crystal with AMP and Asp, 8,2 mg ml^{-1} for crystal with AMP, in 20 mM HEPES buffer pH 7.5, 100 mM NaCl, 1 mM $MgCl_2$, 1% glycerol) containing either 10 mM AMP or 10 mM AMP with 1 mM sodium aspartate, and (ii) a precipitant solution containing 100 mM MES pH 6.5, 0.6 M NaCl and 18% (for crystal with AMP and Asp) or 20% (crystal with AMP) polyethylene glycol (PEG) 4000. Crystals were transferred to a cryoprotectant solution composed of the mother liquor supplemented with 20% PEG 400 and flash-frozen in liquid nitrogen. Diffraction data were collected at 100 K on the PROXIMA 1 and 2 beamlines at the SOLEIL synchrotron (https://www.synchrotron-soleil.fr/en). Intensities were integrated using the XDS program (Kabsch, 2010) and further reprocessed by Staraniso (Tickle *et al.*, 2016). Data quality was assessed using the correlation coefficient $CC_{1/2}$ (Karplus and Diederichs, 2012) (Supplementary Table S4). Crystal structures were determined by performing molecular replacement with Phaser (McCoy *et al.*, 2007) using the structure of AtGH3.5 (PDB 5KOD, Westfall *et al.*, 2016) as a search model. Models were refined with non-crystallographic symmetry restraints and torsional local symmetry using Buster 2.10 (Bricogne *et al.*, 2011) and with ligand occupancies set to 1. Electron density maps were evaluated using COOT (Emsley and Cowtan, 2004). MolProbity was used for structure validation (Chen *et al.*, 2010). Molecular graphics images were generated using PYMOL v 3.0 (www.pymol.org). Ligand interactions were analysed using Discovery Studio Visualizer (BIOVIA, San Diego, CA, USA).

Docking of Asp/Glu conjugates into the active site of AtGH3.6 and AtGH3.5

In silico docking was performed to compare the binding of Asp/Glu and their IAA and PAA conjugates into the active site of AtGH3.6 (PDB 9FXD, this work) and AtGH3.5 (PDB 5KOD, Westfall *et al.*, 2016) by FLARE v 8.0 (Cheeseright *et al.*, 2006; Bauer and Mackey, 2019; CRESSET, http://www.cresset-group.com/flare/). The proteins were prepared for docking using rule-based protonation predicted for pH 7.0 and intelligent capping. Energy grids for docking were 20×20×20 Å in dimension and centred on the amino group of co-crystallized aspartate ligand in the structure AtGH3.6. Docking calculations were carried out by the Lead Finder docking algorithm, with three independent docking runs and keeping the best poses overall (Kuhn *et al.*, 2020). The resulting ligand orientations and conformations were scored based on their binding free energies and the Lead Finder rank score (Stroganov *et al.*, 2008).

Microscale thermophoresis affinity measurements

The microscale thermophoresis (MST) method was used to determine the binding affinity of various amino acids, adenylyl-imidodiphosphate (AMP-PNP), and AMP as well as IAA and PAA ligands. Proteins were fluorescently labelled with RED-tris-NTA dye (Nanotemper Technologies, Munich, Germany) using a 1:1 dye/protein molar ratio. The labelled protein was adjusted to 100 nM in 50 mM MES buffer pH 6.5, 1 mM $MgCl_2$, and 0.05% Tween. Measurements were performed in premium capillaries on a Monolith NT.115 instrument at 30 °C with 5 s/30 s/5 s laser off/on/off times (medium MST power), respectively, with continuous sample fluorescence recording.

Results

Phenylacetyl-glucose is an endogenous phenylacetic acid metabolite synthesized by UGT84B1 and UGT74D1 glucosyltransferases

To determine PAA conjugates, we adopted and modified a method previously developed and applied for IAA metabolite profiling (Hladík *et al.*, 2023). Having this dependable analytical method, we systematically screened for PAA conjugates across various species of land plants. Remarkably, we uncovered the presence of endogenous PAA-glc, a compound previously undetected in plants, within three species: Arabidopsis,

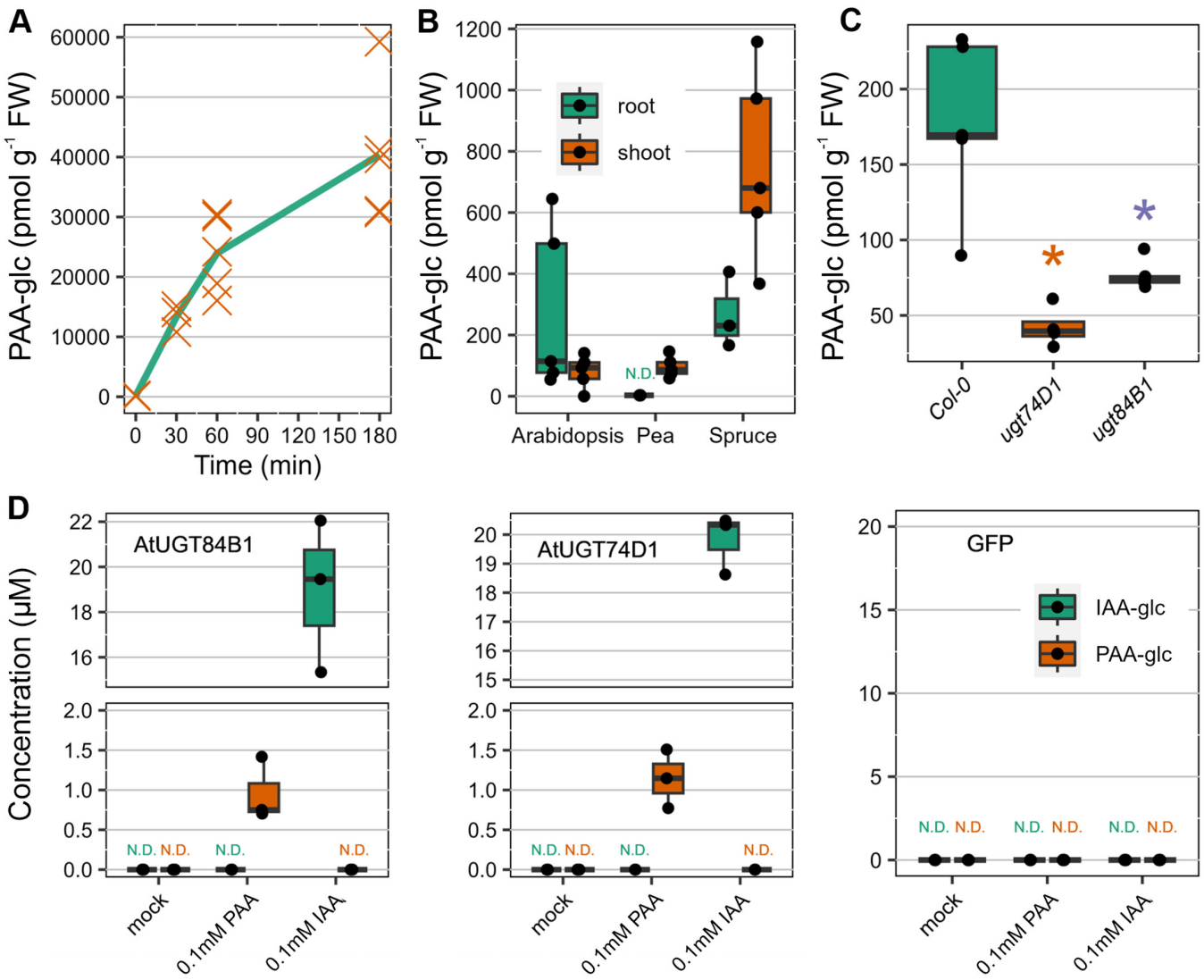

Fig. 1. Presence and formation of PAA-glc in plants. (A) Concentration (pmol g^{-1} FW) of PAA-glc after treatment of Arabidopsis with 20 μM PAA for 30, 60, and 180 min. Each orange cross represents an individual biological replicate (n=5). (B) Endogenous levels of PAA-glc (pmol g^{-1} FW) in roots and shoots of Arabidopsis, pea, and spruce. (C) Levels of PAA-glc (pmol g^{-1} FW) in Col-0, *ugt74d1* and *ugt84b1* knockout Arabidopsis lines. (D) Analysis of IAA-glc and PAA-glc (μM) synthesized by recombinant AtUGT84B1 and AtUGT47D1 produced by a bacterial assay. The cell lysate was incubated with 0.1 mM IAA or PAA and UGT cofactors for 5 h at 30 °C. Cell lysate without treatment was used as a mock sample. The box plots show the upper and lower quartiles, with the horizontal line indicating the median, and each dot representing a single biological replicate. GFP-producing bacteria supplemented with PAA-AAs were used as controls. Statistically significant differences are indicated by asterisks, as determined by Student's t-test ($P \leq 0.05$). All plant profiling was performed in five biological replicates (n=5) and bacterial enzyme assays in three biological replicates (n=3). AA, amino acid; GFP, green fluorescent protein; IAA, indole-3-acetic acid; N.D., not detected; PAA, phenylacetic acid; UGT, UDP-glucosyltransferase.

pea, and spruce. To ensure the identity of endogenous PAA-glc, we compared its chromatographic retention times from Arabidopsis root extracts with that of synthetic PAA-glc standard and with Arabidopsis extracts spiked with 10 pmol of reference standard (Supplementary Fig. S1). Subsequently, to further confirm the formation of PAA-glc *in planta*, we treated Arabidopsis seedlings with 20 μM PAA, and PAA-glc levels were subsequently determined after 30, 60, and 180 min intervals (Fig. 1A). Notably, the concentration of PAA-glc progressively increased from ~180 pmol g^{-1} to 40 nmol g^{-1} FW after 180 min of treatment, demonstrating the *de novo* synthesis of PAA-glc in response to exogenous application of PAA.

The quantitative tissue-specific analysis revealed highest levels of PAA-glc in spruce shoots (almost 760 pmol g^{-1} FW). Levels of around 270 pmol g^{-1} FW were determined in spruce and Arabidopsis roots. Pea and Arabidopsis shoots contained 95 and 80 pmol g^{-1} FW, respectively. In other tissues and species (maize, wheat, and *P. patens*) PAA-glc was not detected (Fig. 1B; Table 1).

Table 1. PAA conjugate levels in various plant species

Species	Tissue	PAA	PAA-Asp	PAA-Glu	PAA-glc
Arabidopsis	Shoot	310.2±23.2	581.0±156.0	507.4±130.0	80.2±54.1
	Root	590.8±273.6	1896.9±906.7	1928.5±868.9	277.8±274.0
Maize (*Zea mays*)	Shoot	<LOD	9.1±2.6	10.2±2.5	<LOD
	Cotyledon	422.3±59.5	25.4±21.9	<LOD	<LOD
	Root	185.1±21.4	50.8±7.3	99.5±27.5	<LOD
Wheat (*Triticum aestivum*)	Shoot	493.0±98.8	16.9±2.2	<LOD	<LOD
	Cotyledon	695.4±504.9	432.4±277.1	16.7±11.5	<LOD
	Root	341.0±112.3	523.5±345.3	<LOD	<LOD
Pea (*Pisum sativum*)	Shoot	1113.5±304.8	1444.7±466.8	54.1±7.8	95.2±34.3
	Cotyledon	310.2±62.3	$37.1\times10^3\pm12.8\times10^3$	1719.9±413.8	<LOD
	Root	1345.0±169.6	1095.4±990.8	272.1±53.6	<LOD
Spruce (*Picea abies*)	Shoot	36.6±13.2	1.6±0.7	5.8±0.3	755.7±311.9
	Root	76.5±18.6	1.9±0.4	2.1±0.2	267.8±124.2
Physcomitrium patens	Gametophores	82.6±36.1	1.8±0.3	27.3±3.5	<LOD

Values are mean ±SD (pmol g^{-1} FW). PAA conjugates were quantified (pmol g^{-1} FW ±SD; n=5) in roots, shoots, and cotyledons of pea, wheat, and maize, roots and shoots of Arabidopsis and spruce, and gametophores of *P. patens*. <LOD, under the limit of detection; PAA, phenylacetic acid; PAA-Asp, phenylacetyl-aspartate; PAA-glc, phenylacetyl-glucose; PAA-Glu, phenylacetyl-glutamate.

The glucosyltransferase UGT84B1 has been identified to be responsible for forming IAA-glc and PAA-glc *in vitro* (Aoi *et al.*, 2020a). Similarly, UGT74D1 has been linked to the formation of oxIAA-glc (Tanaka *et al.*, 2014; Brunoni *et al.*, 2019; Mateo-Bonmatí *et al.*, 2021), although its involvement in PAA metabolism has not been explored. To investigate whether these enzymes are involved in PAA-glc formation, we tested the conjugation activity of these enzymes by expressing them in *E. coli* and using a bacterial assay designed to study various IAA catabolic enzymes (Brunoni *et al.*, 2019, 2023). Both UGT84B1 and UGT74D1 recombinant proteins showed the capability to produce IAA-glc and PAA-glc after exposure to 0.1 μM IAA and PAA, respectively (Fig. 1D). However, the activity of both glucosyltransferases towards PAA was only about 5% compared with IAA. To confirm their activity in plants, we explored PAA-glc content in Arabidopsis knockout lines *ugt84b1* and *ugt74d1*. Remarkably, we observed significantly lower levels of PAA-glc in both mutants compared with Col-0 (Fig. 1C). In conclusion, both experiments demonstrated involvement of UGT84B1 and UGT74D1 in PAA glucosylation.

Exploring novel phenylacetic acid amide conjugates, their enzymatic synthesis and breakdown

Conjugates of IAA with various amino acids have been previously determined in plants. However, the only known amide conjugates of PAA in plants are those linked with Asp, Glu, and Trp (Sugawara *et al.*, 2015; Staswick *et al.*, 2017). In this study, in addition to identifying PAA-glc, we uncovered three previously unreported amide conjugates, PAA-Leu, PAA-Phe, and PAA-Val, in pea and wheat. The verification of newly identified endogenous conjugates relied on comparing their chromatographic retention times with those of synthetic standards, as well as by comparing their fragmentation spectra (Supplementary Figs S2A, B, S3A, B). While endogenous steady-state levels of PAA-Leu, PAA-Phe, PAA-Trp, and PAA-Val in Arabidopsis were below the detection limits, feeding plants with 20 μM PAA promoted their *de novo* synthesis, resulting in detectable endogenous concentrations ranging from 0.5 to 1 pmol g^{-1} FW already after 30 min (Fig. 2A).

PAA-Leu, PAA-Phe, PAA-Val, and PAA-Trp were then quantified in different tissues of various plant species, with detectable concentrations observed only in pea and wheat (Fig. 2B). Pea cotyledons contained all four conjugates in concentrations ranging from 0.5 to 8 pmol g^{-1} FW. PAA-Phe, PAA-Val, and PAA-Leu were detected in roots, and PAA-Phe and PAA-Val were also found in shoots, all in concentrations below 2 pmol g^{-1} FW. All of them were identified in wheat cotyledon at concentrations not exceeding 2 pmol g^{-1} FW.

Previous works showed the involvement of IAA-conjugating GH3 enzymes in the metabolic regulation of PAA (Staswick *et al.*, 2005; Westfall *et al.*, 2016; Aoi *et al.*, 2020c). To investigate the spectrum activity of GH3 enzymes to form PAA amino acid conjugates, recombinant AtGH3.6 and AtGH3.17 enzymes were tested with PAA using a bacterial assay (Fig. 2C). In the presence of 0.1 μM PAA, both enzymes formed all tested PAA amino acid conjugates. Nonetheless, AtGH3.6 predominantly conjugated PAA with Asp and AtGH3.17 with Glu.

Several IAA-AAs can be hydrolysed by members of the ILR1/ILL family, thus contributing to the free IAA pool in addition to *de novo* synthesis (LeClere *et al.*, 2002; Rampey *et al.*, 2004; Hayashi *et al.*, 2021). To investigate whether PAA-AAs could undergo a similar level of regulation, we tested the possible hydrolysing activity of recombinant AtILL2, AtILL6, AtILR1, and AtIAR3 enzymes with 0.1 mM PAA-Leu, PAA-Val, PAA-Trp, or PAA-Glu and followed the formation of PAA (Fig. 2D). GFP-producing bacteria

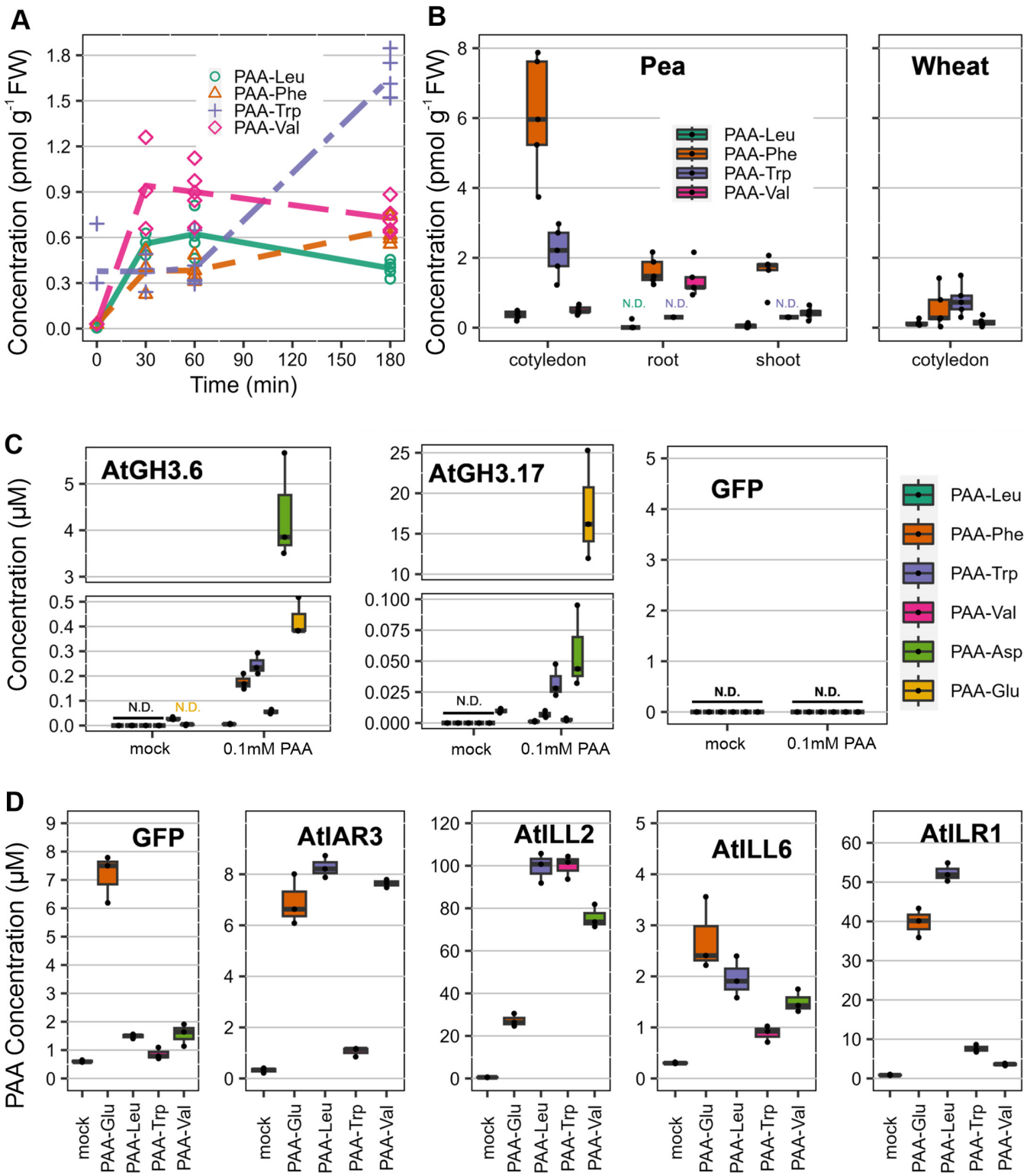

Fig. 2. PAA amide conjugates abundance, formation and hydrolysis. (A) Concentration levels (pmol g^{-1} FW) of PAA-Leu, PAA-Phe, PAA-Trp, and PAA-Val measured in Arabidopsis seedlings after treatment with 20 μM PAA for 30, 60, and 180 min. Each sign in a specific colour represents an individual biological replicate (n=5). (B) Quantification of PAA-Leu, PAA-Phe, PAA-Trp, and PAA-Val (pmol g^{-1} FW) carried out in pea cotyledons, roots, and shoots, as well as in wheat cotyledons. (C) Analysis of PAA-AAs synthesized by recombinant AtGH3.6 and AtGH3.17 performed by a bacterial assay. The cell lysate was incubated with 0.1 mM PAA and GH3 cofactors for 5 h at 30 °C, and the formation of PAA-AAs (μM) was determined. As a control, cell lysate without PAA treatment was used. (D) Hydrolysis of PAA-AAs to PAA examined using a bacterial assay with recombinant AtIAR3, AtILL2, AtILL6, and

AtILR1. The lysate was incubated with 0.1 mM PAA-Leu, PAA-Trp, PAA-Val, and PAA-Glu for 5 h at 30 °C, and the levels of PAA (μM) were measured. A negative control was performed using GFP-producing bacteria, and a mock was performed using cell lysate without treatment. The box plots display the median as a horizontal line, upper and lower quartiles as the box, and each dot represents a single biological replicate. All plant profiling was performed in five biological replicates (n=5) and bacterial enzyme assays in three biological replicates (n=3). AA, amino acid; GFP, green fluorescent protein; GH3, GRETCHEN HAGEN 3; IAR3, IAA-ALANINE RESISTANT 3; ILL, ILR1-LIKE protein; ILR1, IAA-LEUCINE RESISTANT 1; N.D., not detected; PAA, phenylacetic acid.

supplemented with PAA-AAs were used as controls. AtIAR3 preferentially hydrolysed PAA-Glu/-Leu/-Val, while AtILL6 did not exhibit any clear substrate preference. However, the amount of PAA formed by these enzymes was comparable with the GFP control, indicating the presence of endogenous substrate-associated machinery in *E. coli*, and thus AtIAR3 and AtILL6 may not significantly contribute to the hydrolysis of these PAA amino acid conjugates. AtILL2 showed a pronounced preference for hydrolysing PAA-Leu/-Trp/-Val, while AtILR1 preferably hydrolysed PAA-Glu and PAA-Leu. Overall, our findings demonstrate the capability of ILR/ILL proteins to hydrolyse PAA amino acid conjugates.

Crystal structures determination and docking of amino acids with GRETCHEN HAGEN 3s

Available crystal structures of AtGH3.6 with inhibitor (PDB 7VKA; Xie *et al.*, 2022), AtGH3.5 with IAA (PDB 5KOD; Westfall *et al.*, 2016), AtGH3.12 (PDB 4EPM and 4EQL, the latter containing salicylate; Westfall *et al.*, 2012) and AtGH3.15 (PDB 6AVH; Sherp *et al.*, 2018) contain AMP (as a product of ATP degradation) but not a free amino acid entering the ligase reaction with the second substrate (IAA/PAA). To understand the basis for amino acid specificity in GH3s, we solved the crystal structure of AtGH3.6 in the presence of AMP only or AMP together with aspartate, up to 1.74 Å resolution. Data collection and refinement statistics are in Supplementary Table S4. Superposition of both structures did not reveal rearrangement in the presence of amino acid (aspartate) ligand in the active site. The α-amino group of aspartate interacts with the phosphate group of AMP. The α-carboxyl group is H-bonded to the nitrogen atom of Leu175 and via two water molecules to the hydroxyl of Thr176 and main-chain oxygen of Phe158 (Fig. 3A). Moreover, both α-carboxyl and α-amino groups interact via a water molecule with Ser341 and the oxygen atom of Thr108. The γ-carboxyl group is bound to Arg117, Lys160, and Ser455. Binding affinities for AtGH3.6 were analysed by MST. K_D values for Glu and Asp were 0.72 mM and 0.68 mM, respectively (Fig. 3B). Binding of Val and Leu was not measurable by MST. Affinities for IAA and PAA were similar and at around 60 μM concentration. The superposition of AtGH3.6 with AtGH3.5 shows the conservation of the amino acid binding site and, thus, similar specificity (Fig. 3C).

Our attempts to obtain structures with bound products IAA-Asp or PAA-Asp were unsuccessful due to solubility issues of these ligands and a loss of crystal diffraction upon co-crystallization with AtGH3.6. Thus, we docked these two compounds as well as the amino acids in the active site of AtGH3.6 and AtGH3.5 by FLARE v 8.0 (Cheeseright *et al.*, 2006; Bauer and Mackey, 2019; CRESSET, http://www.cresset-group.com/flare/) using the Lead Finder (LF) docking algorithm (Supplementary Table S5). The LF ranking score and Gibbs free energy (ΔG) score for Asp and Glu were similar and mutually comparable, confirming their similar affinities observed by MST. The ΔG score estimates the free energy of protein–ligand binding for a given protein–ligand complex. Similar LF ranking scores were obtained for the IAA- and PAA-conjugates with Asp/Glu in line with similar affinities for IAA/PAA measured by MST. The best positions for IAA-Asp and PAA-Asp in the AtGH3.6 site are shown in Fig. 3D.

Phenylacetic acid conjugates profiling in land plants

While previous studies have extensively examined PAA levels across various plant species and tissues (reviewed in Perez *et al.*, 2023), information regarding its conjugate levels is mainly restricted to Arabidopsis (Sugawara *et al.*, 2015; Aoi *et al.*, 2020c). Therefore, we conducted a thorough tissue-specific profiling encompassing high-abundance PAA conjugates, namely PAA-Asp, PAA-Glu, and PAA-glc, across diverse plant species of land plants (Table 1). Intriguingly, we observed significant variations in the PAA conjugate profile among species and even within tissues.

Remarkably, spruce and *P. patens* exhibited lower levels of free PAA and PAA-Asp than the representative angiosperms. Additionally, spruce represented the only species where the predominant conjugate was PAA-glc, accounting for around 95% of shoot PAA pool. Among other species, amide conjugates were more abundant. In moss, the level of PAA-Glu was more than 10 times higher than PAA-Asp, unlike in all other species. In both monocots, maize and wheat, the cotyledons accumulated PAA the most. PAA-glc was not detected in these species. In Arabidopsis, most of the PAA conjugates were present in roots, primarily in the form of PAA-AAs. However, notable levels of free PAA and PAA-glc were also detected. In pea, PAA-Asp was the predominant storage form, with concentrations reaching approximately 40 nmol g^{-1} in cotyledons. Overall, pea stores a considerable amount of PAA in amide form.

Metabolic pathways of phenylacetic acid display only partial functional redundancy

Previous studies have demonstrated the presence of functional redundancy within pathways of IAA metabolism (Mellor *et al.*,

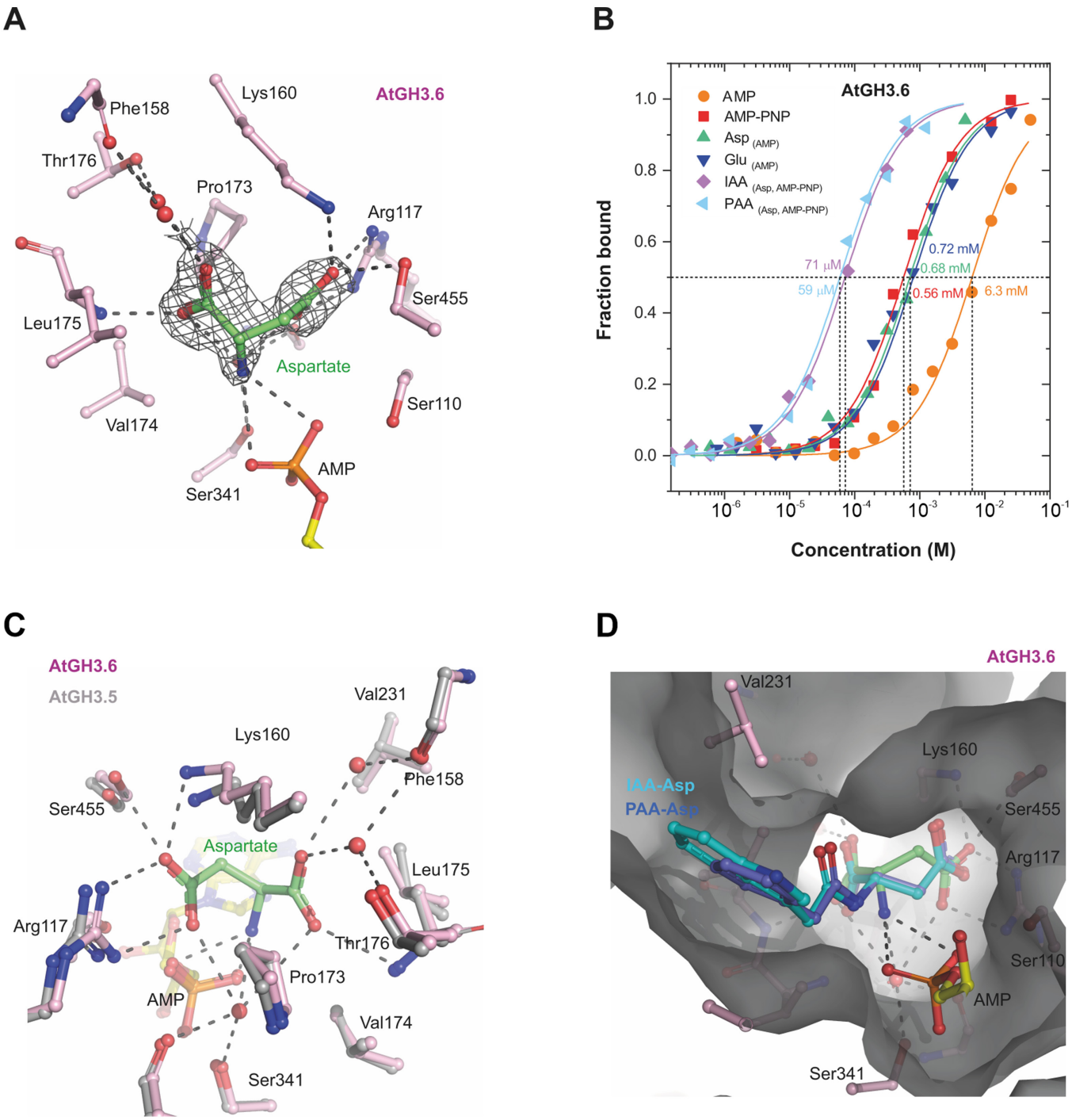

Fig. 3. Binding interactions of aspartate in the active site of AtGH3.6. (A) Binding of Asp (coloured in green) in AtGH3.6. Surrounding residues are coloured pink and labelled. Ligand is depicted in its annealing Fo–Fc omit map (black mesh) contoured at 3.5 σ (PDB 9FXD). (B) Binding affinity curves of AtGH3.6 for selected ligands, AMP, AMP-PNP, Glu, Asp, IAA-Asp and PAA-Asp. Data were measured by MST in 50 mM MES buffer pH 6.5, 1 mM $MgCl_2$, and 0.05% Tween. (C) Superposition of the amino acid binding site of AthGH3.6 (coloured pink, PDB 9FXD) with AtGH3.5 structure (coloured grey, PDB 5KOD). (D) Docked positions of IAA-Asp and PAA-Asp in the active site of AtGH3.6. Docking calculation was performed by FLARE v 8.0. AMP-PNP, adenylyl-imidodiphosphate; IAA, indole-3-acetic acid; GH3, GRETCHEN HAGEN 3; MST, microscale thermophoresis; PAA, phenylacetic acid.

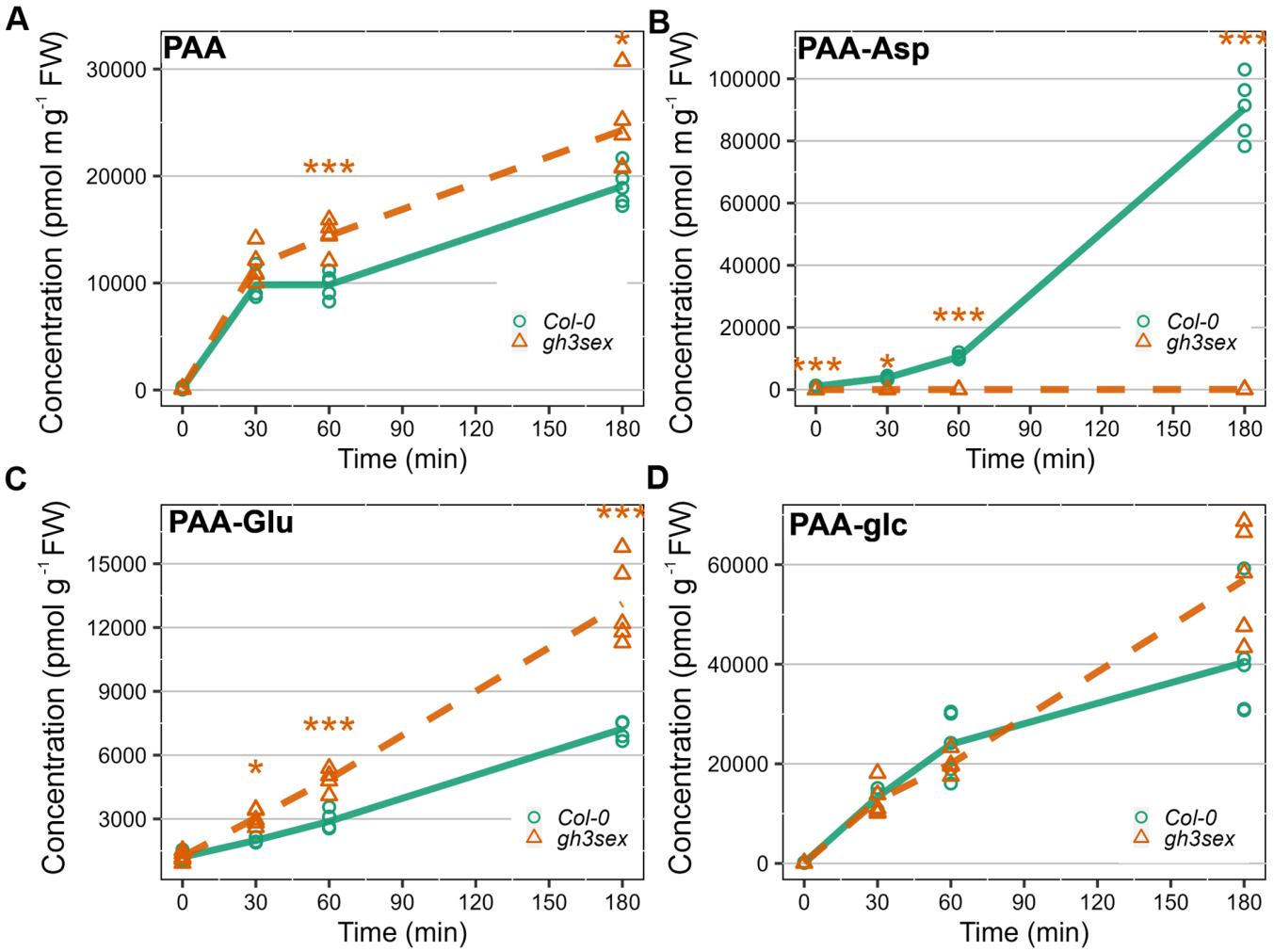

Fig. 4. PAA metabolism in Arabidopsis gh3sex knockout mutant. Arabidopsis line *gh3.1*, *2*, *3*, *4*, *5*, *6* (*gh3sex*) and Columbia (Col-0) were treated with 20 μM PAA for 30, 60, and 180 min. The concentrations levels (pmol g^{-1} FW) of PAA (A), PAA-Asp (B), PAA-Glu (C), and PAA-glc (D) were measured at those four time points. Each sign in a specific colour represents an individual biological replicate (n=5). Asterisks indicate statistically significant differences between the Col-0 and mutant line at one time point, as determined by Student's t-test (*$P \leq 0.05$, **$P \leq 0.01$, ***$P \leq 0.001$). The colour of the asterisk corresponds to the mutant line that is significantly different from Col-0. PAA, phenylacetic acid.

2016; Porco *et al.*, 2016). Here, we aimed to investigate the dynamic changes in PAA and its conjugates in response to perturbations in specific metabolic pathways, providing insights into the mechanisms governing PAA homeostasis.

Arabidopsis *gh3sex* mutant seedlings, affected in the GH3-dependent PAA-AA synthesis, were treated with 20 μM PAA for 30, 60, and 180 min, and the levels of PAA amide conjugates were compared with wild type (Col-0). The PAA levels immediately increased after treatment, suggesting rapid uptake of exogenously applied PAA by plants (Fig. 4A). Subsequent analysis at 60 min post-treatment revealed significant differences in PAA concentrations between the *gh3sex* and Col-0 lines. Notably, while wild-type plants accumulated PAA-Asp over time, no PAA-Asp was detected in the mutant throughout the experiment (Fig. 4B), highlighting the dominant role of AtGH3.1-6 enzymes in the conjugation of PAA with Asp. The PAA-Glu levels were elevated in the *gh3sex* mutant at 60 min and 180 min post-treatment (Fig. 4C). The increase in PAA-Glu levels in mutant could be attributed to compensatory mechanisms and functional redundancy of GH3 proteins (Porco *et al.*, 2016; Brunoni *et al.*, 2023). Measurement of PAA-glc levels did not reveal any significant differences between wild type and mutant (Fig. 4D).

To compare PAA metabolism across phylogenetically diverse plant species, we employed the synthetic GH3 inhibitor KKI, known for inhibiting the formation of IAA-AAs (Fukui *et al.*, 2022). Anticipating a similar function in PAA metabolism, we investigated its effects in Arabidopsis, spruce, and *P. patens*, by treating them with 50 μM KKI, 5 μM PAA, or a combination of both.

In Arabidopsis, co-treatment with PAA and KKI resulted in reduced levels of PAA-Asp and PAA-Glu compared with PAA

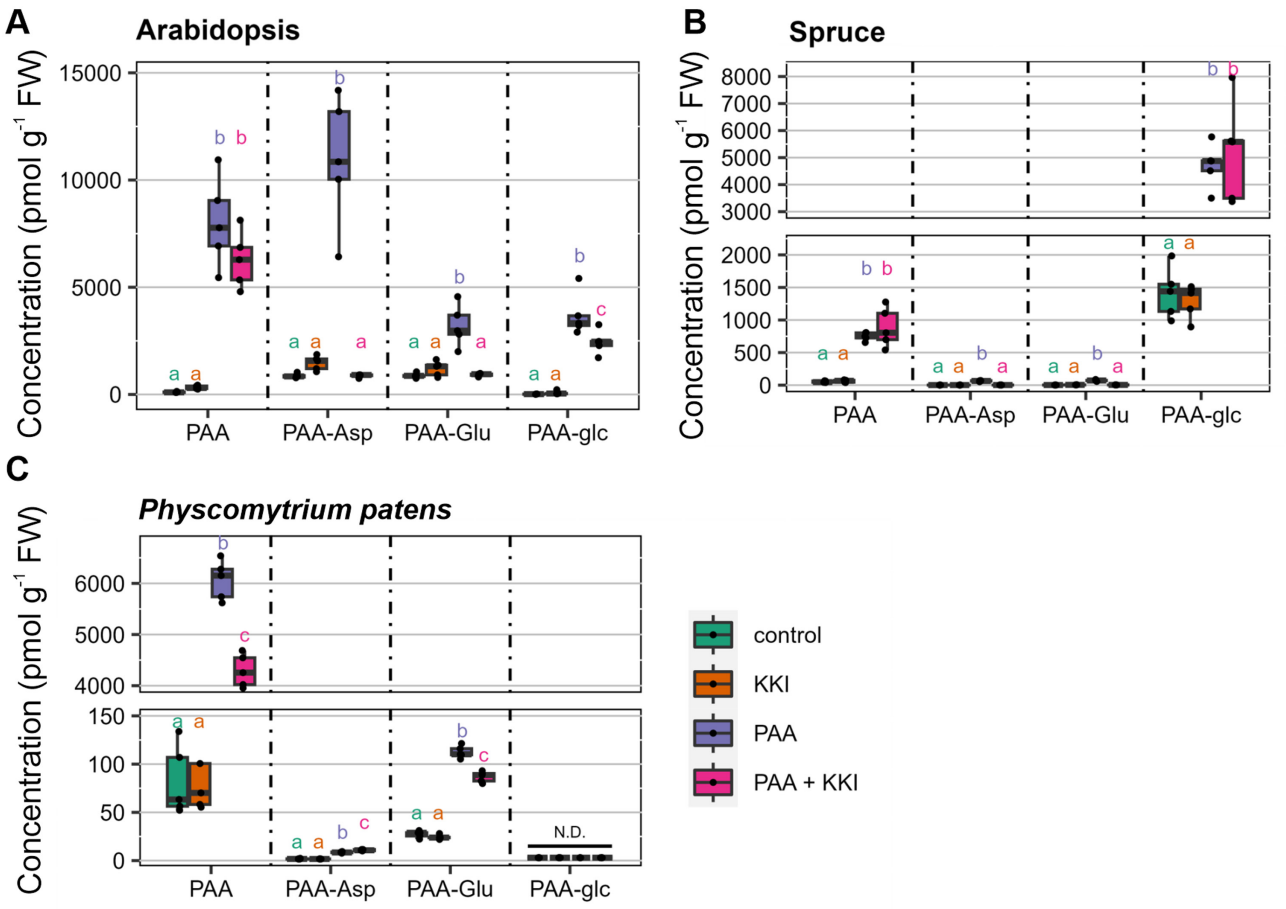

Fig. 5. PAA metabolism after PAA and KKI treatment in various plant species. Arabidopsis (A), spruce (B), and *Physcomitrium patens* (C) were treated with 50 μM KKI, 5 μM PAA or their combination for 1, 6, or 24 h, respectively, with time depending on the species. The concentration (pmol g^{-1} FW) of PAA, PAA-Asp, PAA-Glu, and PAA-glc was measured after the treatment. As a control, mock treated samples were used. The box plots display the median as a horizontal line, upper and lower quartiles as the box, and each dot represents a single biological replicate (n=5). One-way ANOVA and Tukey's post-hoc test were applied to assess the differences between treatment groups. Different letters (a–c) indicate significant differences at the 5% level of significance (P≤0.05). The colour of the letters corresponds with the colour of the boxplot. KKI, kakeimide; N.D., not detected; PAA, phenylacetic acid.

treatment alone, confirming the activity of KKI in inhibiting PAA-AA formation. Interestingly, levels of free PAA remained unchanged between the two treatments (Fig. 5A). In spruce, the treatment with PAA confirmed a predominant role of glucosylation in PAA metabolism. In agreement to Arabidopsis, KKI inhibited the GH3-mediated formation of both amide conjugates (Fig. 5B). Interestingly, in *P. patens*, only formation of PAA-Glu was blocked by KKI in co-treatment with PAA, while the PAA-Asp level was elevated (Fig. 5C). Notably, the formation of PAA-glc was not observed even after PAA treatment, suggesting that glucosylation does not occur in PAA metabolism in *P. patens*.

Discussion

Metabolism plays a pivotal role in maintaining auxin homeostasis, by ensuring optimal levels of biologically active hormone within the plant. While extensive research governing IAA metabolism has been done in previous years (Brunoni *et al.*, 2020, 2023; Hayashi *et al.*, 2021; Mateo-Bonmatí *et al.*, 2021; Müller *et al.*, 2021; Hladík *et al.*, 2023), the inactivation pathways of PAA remain largely uncharacterized. Thus far, only PAA-Asp, PAA-Glu, and PAA-Trp have been identified in Arabidopsis (Sugawara *et al.*, 2015; Staswick *et al.*, 2017). However, there is no evidence about other conjugates or metabolic pathways, as oxidation of the phenyl ring is unlikely and the formation of a glucosyl ester (PAA-glc) has only been demonstrated *in vitro* (Aoi *et al.*, 2020a).

In our study we aimed to broaden the understanding of PAA metabolism by investigating novel conjugates and metabolic pathways (Fig. 6). As a result of comprehensive multi-species screening, we confirmed the occurrence of four novel PAA conjugates, PAA-glc, PAA-Leu, PAA-Phe, and PAA-Val, in different plant species. The identity of endogenous conjugates was

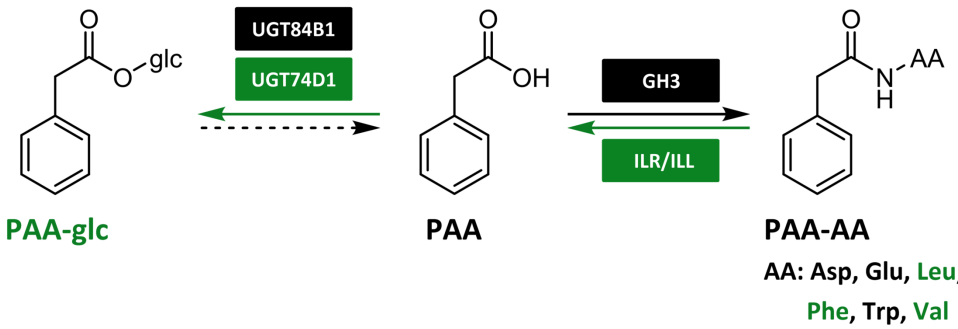

Fig. 6. Updated scheme of PAA metabolism. Newly identified pathways and conjugates are highlighted in green. Dashed arrow represents putative metabolic step that is still not fully characterized. AA, amino acid; GH3, GRETCHEN HAGEN 3; ILR/ILL, IAA-LEUCINE RESISTANT 1/ILR1-LIKE proteins; PAA, phenylacetic acid; PAA-glc, PAA-glucose.

confirmed by comparison of their retention times with that of synthetic standards under the same chromatographic conditions. PAA-glc was found in Arabidopsis, pea and spruce, in concentrations ranging from 50 to 1000 pmol g^{-1} FW, with the highest levels observed in spruce shoots (Fig. 1B). However, even these high levels were close to the limit of detection of our method, likely due to poor ionization of the molecule. It is plausible that PAA-glc may also be present in other studied species, but below the limit of detection. The presence of newly identified amide conjugates, PAA-Leu, PAA-Phe, and PAA-Val, was observed only in pea and wheat in low concentrations ranging from 0.5 to 8 pmol g^{-1} FW (Fig. 2B). These findings align with the low levels of IAA and oxIAA conjugates with amino acids other than Asp and Glu quantified previously in various plants (Kowalczyk and Sandberg, 2001; Pěnčík *et al.*, 2009; Hladík *et al.*, 2023). While Staswick *et al.* (2017) observed high levels of PAA-Trp (approximately 30 pmol g^{-1} FW) in Arabidopsis tissue, under our experimental conditions PAA-Trp was not detected in Arabidopsis, being only determined in pea and wheat cotyledons. Although PAA conjugates with Leu, Phe, Trp, and Val were not found in Arabidopsis, the capability of Arabidopsis GH3 proteins to catalyse their synthesis was proved by a bacterial enzymatic assay (Fig. 2C). To further validate the formation of newly identified metabolites *in planta*, we conducted feeding experiments by supplying exogenous PAA to Arabidopsis seedlings. This led to rapid synthesis of PAA-glc (Fig. 1A) as well as all three novel amide conjugates (Fig. 2A), underscoring the role of these conjugates in maintaining PAA homeostasis.

Formation of PAA-glc by enzyme UGT84B1 has already been shown *in vitro* (Aoi at el., 2020c). However, other glucosyltransferases can also be involved in formation of IAA/oxIAA-glc, such as UGT74D1 (Jackson *et al.*, 2001; Brunoni *et al.*, 2019; Mateo-Bonmatí *et al.*, 2021). Thus, we tested the conjugation activity of this protein in a bacterial assay designed to study IAA enzymatic inactivation (Brunoni *et al.*, 2019, 2023) and proved the capability of AtUGT74D1 to produce PAA-glc (Fig. 1D). Additionally, we quantified PAA-glc in *ugt84b1* and *ugt74d1* knockouts and demonstrated the involvement of both proteins in formation of PAA-glc *in planta* (Fig. 1C). Notably, PAA levels displayed no significant difference between the mutants and the wild type. This finding aligns with the expectation that PAA homeostasis is regulated by multiple metabolic pathways. The observed reduction in PAA-glc levels in *ugt74d1* and *ugt84b* does not necessarily result in an increase in free PAA, likely due to compensatory metabolic mechanisms.

The GH3-mediated formation of IAA amide conjugates is a well described mechanism (Staswick *et al.*, 2005; Zhang *et al.*, 2018). The role of GH3s in PAA metabolism was also indicated for PAA-Asp and PAA-Glu formation (Sugawara *et al.*, 2015; Westfall *et al.*, 2016; Aoi *et al.*, 2020c). To investigate the role of GH3s in formation of other PAA-AAs, we performed bacterial enzyme assays with AtGH3.6 and AtGH3.17 (Fig. 2C). Results indicated that both GH3 proteins are capable of synthesizing all tested PAA conjugates, with AtGH3.6 displaying a preference for Asp and AtGH3.17 for Glu as substrates, aligning with previous assays with IAA conjugation (Brunoni *et al.*, 2019, 2023). Accordingly, the crystal structure of AtGH3.6 in the presence of Asp (PDB 9FXD) indicates hydrogen bonding of the Asp side chain with three protein residues (Arg117, Lys160, Ser455), favouring Asp binding (Fig. 3). Of note, superposition of a 9FXD structure with that of AtGH3.5 with bound AMP and IAA (PDB 5KOD) shows that these three conserved residues are positioned similarly, favouring Asp binding. Final activity and thus specificity depends not only on affinities but also on transition state stability and association and dissociation rate of the enzyme–substrate complex plus availability of particular ligands, which can lead to differences among GH3 family enzymes among various species. Furthermore, we investigated the putative hydrolysis of PAA-AAs by ILR/ILL amidohydrolases (Fig. 2D), as previously described for IAA conjugates (Bartel and Fink, 1995; Davies *et al.*, 1999; LeClere *et al.*, 2002; Hayashi *et al.*, 2021). Bacterial enzyme assays with AtILL2, AtILL6, AtILR1, and AtIAR3 revealed that PAA-AAs can be hydrolysed into free PAA, indicating storage function of PAA amino acid conjugates.

To elucidate evolutionary aspects of PAA metabolism, we conducted profiling of PAA and its major conjugates, PAA-Asp,

PAA-Glu, and PAA-glc, across a spectrum of phylogenetically diverse land plants. Our study encompassed representatives such as the moss *P. patens*, spruce as a representative of gymnosperm trees, dicots represented by Arabidopsis and pea, and two monocots, maize and wheat (Table 1).

According to our findings, PAA levels largely align with previous studies, revealing consistent PAA levels in Arabidopsis and pea tissues (Wightman and Lighty, 1982; Sugawara *et al.*, 2015). Notably, comparison with our previous IAA quantifications (Hladík *et al.*, 2023) as well as with earlier reports indicates significantly higher PAA levels in most plant species and tissues. PAA conjugate profiling revealed PAA-AAs as major metabolites across all studied plants except spruce, where PAA-glc concentrations were notably higher compared with PAA amides. This finding, together with results obtained from a PAA feeding experiment (Fig. 5B) and previously reported evidence that IAA glucosylation is the main pathway to maintain IAA homeostasis (Brunoni *et al.*, 2020), suggests that glucosylation serves as the preferred pathway for PAA and IAA inactivation in spruce. Remarkably, the exceptionally high concentrations of PAA-AAs in pea mirror elevated levels of IAA-AAs and oxIAA-AAs in pea tissues (Hladík *et al.*, 2023), suggesting analogous metabolic regulation of both auxins. Although PAA conjugation pathways share similarities with those of IAA, the oxidation to oxIAA that serves as a degradation mechanism of IAA and IAA-AAs (Hayashi *et al.*, 2021) represents a notable difference between IAA and PAA metabolism. Both oxIAA and its glucosyl ester are considerably more abundant among IAA metabolites (Kai *et al.*, 2007a; Pěnčík *et al.*, 2018; Hladík *et al.*, 2023). In contrast, PAA-Asp and PAA-Glu exhibit substantially higher accumulation compared with IAA amide conjugates and represent predominant PAA metabolites in Arabidopsis (Table 1).

To investigate putative functional redundancy in PAA inactivation between GH3s and UGTs, we explored PAA metabolism using GH3-deficient Arabidopsis mutant and the synthetic GH3 inhibitor KKI (Fukui *et al.*, 2022). Following the application of PAA, the synthesis of PAA-Asp was dramatically reduced in *gh3sex* (Fig. 4). This reduction was partially compensated by an increased conjugation of PAA to Glu. Notably, the deficiency in GH3-mediated conjugation was not compensated by glucosylation, mirroring observations seen with IAA (Porco *et al.*, 2016). This observation was further confirmed by the co-treatment of Arabidopsis, spruce, and *P. patens* with PAA and KKI, where no metabolic compensation between GH3s and UGTs was observed (Fig. 5).

In conclusion, our investigation of PAA metabolism has provided valuable insights into the metabolic pathways governing PAA homeostasis in land plants. It appears that there may be other metabolic pathways of PAA that have yet to be discovered, as many have been found in bacteria (Schneider *et al.*, 1997; Navarro-Llorens *et al.*, 2005; Teufel *et al.*, 2010). However, through the identification of novel PAA conjugates and the elucidation of metabolic pathways, we have expanded our understanding of the mechanisms maintaining PAA homeostasis and demonstrated the complexity and species-specific nature of PAA metabolism.

Supplementary data

The following supplementary data are available at *JXB* online.

Fig. S1. Representative multiple reaction monitoring (MRM) chromatograms of PAA-glc.

Fig. S2. PAA-Trp and PAA-Val identification.

Fig. S3. PAA-Leu and PAA-Phe identification.

Table S1. Conditions and parameters of HPLC-MS/MS method.

Table S2. Method validation in Arabidopsis extract.

Table S3. Method validation in pea extract.

Table S4. Data collection and refinement statistics.

Table S5. Ligand lead finder rank (LF) docking score and ΔG (Gibbs free energy) score for selected amino acid substrates and products.

Acknowledgements

We acknowledge Prof. Karin Ljung (Umeå Plant Science Centre, Sweden) for seeds of Arabidopsis mutant lines and SOLEIL for providing synchrotron radiation facilities in using PROXIMA 1 and 2 beamlines (proposal ID 20210831).

Author contributions

FB, ON, AP—conceptualization; PH, DK, AP—methodology; PH—validation; PH, PB, DK, AP—formal analysis; PH, FB, AZ, MZ, JB, DK, NF, AP—investigation; PH, DK, PB, AP—data curation; PH, DK, AP—writing (initial draft); FB, AZ, JB, DK, PB, ON—writing (reviewing and editing); ON, AP—Supervision; PB, ON—funding acquisition. All authors contributed to the article and approved the submitted version.

Conflict of interest

The authors declare they have no conflict of interest.

Funding

This work was supported by the project TowArds Next GENeration Crops, of the ERDF Programme Johannes Amos Comenius [grant number CZ.02.01.01/00/22_008/0004581]. The structural part was supported by the Jean d'Alembert fellowship as part of the France 2030 program [grant number ANR-11-IDEX-0003].

Data availability

The atomic coordinates and structure factors have been deposited in the Protein Data Bank (www.wwpdb.org) under accession codes 9FWD for

AtGH3.6 with AMP and 9FXD for AtGH3.6 with AMP and aspartate. The data that support the findings of this study are openly available in Zenodo at https://doi.org/10.5281/zenodo.13587370 (Hladík *et al.*, 2025).

References

Aoi Y, Hira H, Hayakawa Y, Liu H, Fukui K, Dai X, Tanaka K, Hayashi KI, Zhao Y, Kasahara H. 2020a. UDP-glucosyltransferase UGT84B1 regulates the levels of indole-3-acetic acid and phenylacetic acid in Arabidopsis. Biochemical and Biophysical Research Communications **532**, 244–250.

Aoi Y, Oikawa A, Sasaki R, Huang J, Hayashi K, Kasahara H. 2020b. Arogenate dehydratases can modulate the levels of phenylacetic acid in Arabidopsis. Biochemical and Biophysical Research Communications **524**, 83–88.

Aoi Y, Tanaka K, Cook SD, Hayashi KI, Kasahara H. 2020c. GH3 auxin-amido synthetases alter the ratio of indole-3-acetic acid and phenylacetic acid in Arabidopsis. Plant & Cell Physiology **61**, 596–605.

Bartel B, Fink GR. 1995. ILR1, an amidohydrolase that releases active indole-3-acetic acid from conjugates. Science **268**, 1745–1748.

Bauer MR, Mackey MD. 2019. Electrostatic complementarity as a fast and effective tool to optimize binding and selectivity of protein-ligand complexes. Journal of Medicinal Chemistry **62**, 3036–3050.

Bieleszová K, Pařízková B, Kubeš M, *et al*. 2019. New fluorescently labeled auxins exhibit promising anti-auxin activity. New Biotechnology **48**, 44–52.

Boyes DC, Zayed AM, Ascenzi R, McCaskill AJ, Hoffman NE, Davis KR, Görlach J. 2001. Growth stage-based phenotypic analysis of Arabidopsis: a model for high throughput functional genomics in plants. The Plant Cell **13**, 1499–1510.

Bricogne G, Blanc E, Brandl M, *et al*. 2011. BUSTER version 2.1.0. Cambridge, UK: Global Phasing Ltd.

Brunoni F, Collani S, Casanova-Sáez R, Šimura J, Karady M, Schmid M, Ljung K, Bellini C. 2020. Conifers exhibit a characteristic inactivation of auxin to maintain tissue homeostasis. New Phytologist **226**, 1753–1765.

Brunoni F, Collani S, Šimura J, Schmid M, Bellini C, Ljung K. 2019. A bacterial assay for rapid screening of IAA catabolic enzymes. Plant Methods **15**, 126.

Brunoni F, Pěnčík A, Žukauskaitė A, Ament A, Kopečná M, Collani S, Kopečný D, Novák O. 2023. Amino acid conjugation of oxIAA is a secondary metabolic regulation involved in auxin homeostasis. New Phytologist **238**, 2264–2270.

Casanova-Sáez R, Mateo-Bonmatí E, Ljung K. 2021. Auxin metabolism in plants. Cold Spring Harbor Perspectives in Biology **13**, a039867.

Cheeseright T, Mackey M, Rose S, Vinter A. 2006. Molecular field extrema as descriptors of biological activity: definition and validation. Journal of Chemical Information and Modeling **46**, 665–676.

Chen VB, Arendall WB 3rd, Headd JJ, Keedy DA, Immormino RM, Kapral GJ, Murray LW, Richardson JS, Richardson DC. 2010. MolProbity: all-atom structure validation for macromolecular crystallography. Acta Crystallographica, Section D: Biological Crystallography **66**, 12–21.

Cohen JD, Strader LC. 2024. An auxin research odyssey: 1989-2023. The Plant Cell **36**, 1410–1428.

Cook SD. 2019. An historical review of phenylacetic acid. Plant & Cell Physiology **60**, 243–254.

Cook SD, Nichols DS, Smith J, Chourey PS, McAdam EL, Quittenden L, Ross JJ. 2016. Auxin biosynthesis: Are the indole-3-acetic acid and phenylacetic acid biosynthesis pathways mirror images? Plant Physiology **171**, 1230–1241.

Davies PJ. 2010. Plant hormones: biosynthesis, signal transduction, action! New York: Springer.

Davies RT, Goetz DH, Lasswell J, Anderson MN, Bartel B. 1999. *IAR3* encodes an auxin conjugate hydrolase from Arabidopsis. The Plant Cell **11**, 365–376.

Emsley P, Cowtan K. 2004. Coot: model-building tools for molecular graphics. Acta Crystallographica, Section D: Biological Crystallography **60**, 2126–2132.

Fukui K, Arai K, Tanaka Y, *et al*. 2022. Chemical inhibition of the auxin inactivation pathway uncovers the roles of metabolic turnover in auxin homeostasis. Proceedings of the National Academy of Sciences, USA **119**, e2206869119.

Gabor EM, Janssen DB. 2004. Increasing the synthetic performance of penicillin acylase PAS2 by structure-inspired semi-random mutagenesis. Protein Engineering, Design & Selection **17**, 571–579.

Graves S, Piepho H, Selzer L, Dorai-Raj S. 2019. multcompView: Visualizations of paired comparisons. R package version 0.1-8/r26. https://R-Forge.R-project.org/projects/multcompview.

Grubb CD, Zipp BJ, Ludwig-Müller J, Masuno MN, Molinski TF, Abel S. 2004. Arabidopsis glucosyltransferase UGT74B1 functions in glucosinolate biosynthesis and auxin homeostasis. The Plant Journal **40**, 893–908.

Haagen-Smit SAJ, Went FW. 1935. A physiological analysis of growth substance. Proceedings Koninklijke Nederlandse Akademie van Wetenschappen **38**, 852–857.

Hayashi K, Arai K, Aoi Y, *et al*. 2021. The main oxidative inactivation pathway of the plant hormone auxin. Nature Communications **12**, 6752.

Hladík P, Brunoni F, Žukauskaitė A, Zatloukal M, Bělíček J, Kopečný D, Briozzo P, Ferchaud N, Novák O, Pěnčík A. 2025. Data from: Phenylacetic acid metabolism in land plants: novel pathways and metabolites. Zenodo. https://doi.org/10.5281/zenodo.13587370

Hladík P, Petřík I, Žukauskaitė A, Novák O, Pěnčík A. 2023. Metabolic profiles of 2-oxindole-3-acetyl-amino acid conjugates differ in various plant species. Frontiers in Plant Science **14**, 1217421.

Hothorn T, Bretz F, Westfall P. 2008. Simultaneous inference in general parametric models. Biometrical Journal. Biometrische Zeitschrift **50**, 346–363.

Iddon L, Richards SE, Johnson CH, Harding JR, Wilson ID, Nicholson JK, Lindon JC, Stachulski AV. 2011. Synthesis of a series of phenylacetic acid 1-β-*O*-acyl glucosides and comparison of their acyl migration and hydrolysis kinetics with the corresponding acyl glucuronides. Organic & Biomolecular Chemistry **9**, 926–934.

Illić N, Magnus V, Ostin A, Sandberg G. 1997. Stable-isotope labeled metabolites of the phytohormone, indole-3-acetic acid. Journal of labelled compounds and radiopharmaceuticals **39**, 433–440.

Jackson RG, Lim EK, Li Y, Kowalczyk M, Sandberg G, Hogget J, Ashford DA, Bowles DJ. 2001. Identification and biochemical characterization of an *Arabidopsis* indole-3-acetic acid glucosyltransferase. The Journal of Biological Chemistry **276**, 4350–4356.

Kabsch W. 2010. XDS. Acta Crystallographica, Section D: Biological Crystallography **66**, 125–132.

Kai K, Horita J, Wakasa K, Miyagawa H. 2007a. Three oxidative metabolites of indole-3-acetic acid from *Arabidopsis thaliana*. Phytochemistry **68**, 1651–1663.

Kai K, Nakamura S, Wakasa K, Miyagawa H. 2007b. Facile preparation of deuterium-labeled standards of indole-3-acetic acid (IAA) and its metabolites to quantitatively analyze the disposition of exogenous IAA in *Arabidopsis thaliana*. Bioscience, Biotechnology, and Biochemistry **71**, 1946–1954.

Kaminaga Y, Schnepp J, Peel G, *et al*. 2006. Plant phenylacetaldehyde synthase is a bifunctional homotetrameric enzyme that catalyzes phenylalanine decarboxylation and oxidation. The Journal of Biological Chemistry **281**, 23357–23366.

Karplus PA, Diederichs K. 2012. Linking crystallographic model and data quality. Science **336**, 1030–1033.

Kawazu K, Zhang H, Yamashita H, Kanzaki H. 1996. Relationship between the pathogenicity of the pine wood nematode, *Bursaphelenchus xylophilus*, and phenylacetic acid production. Bioscience, Biotechnology, and Biochemistry **60**, 1413–1415.

Končitíková R, Vigouroux A, Kopečná M, Andree T, Bartoš J, Šebela M, Moréra S, Kopečný D. 2015. Role and structural characterization of

plant aldehyde dehydrogenases from family 2 and family 7. The Biochemical Journal **468**, 109–123.

Kowalczyk M, Sandberg G. 2001. Quantitative analysis of indole-3-acetic acid metabolites in Arabidopsis. Plant Physiology **127**, 1845–1853.

Kuhn M, Firth-Clark S, Tosco P, Mey ASJS, Mackey M, Michel J. 2020. Assessment of binding affinity via alchemical free-energy calculations. Journal of Chemical Information and Modeling **60**, 3120–3130.

Kunkel BN, Harper CP. 2018. The roles of auxin during interactions between bacterial plant pathogens and their hosts. Journal of Experimental Botany **69**, 245–254.

Lancashire PD, Bleiholder H, Boom PVD, Langeluddeke P, Stauss R, Weber E, Witzenberger A. 1991. A uniform decimal code for growth stages of crops and weeds. Annals of Applied Biology **11**, 561–601.

LeClere S, Tellez R, Rampey RA, Matsuda SPT, Bartel B. 2002. Characterization of a family of IAA-amino acid conjugate hydrolases from *Arabidopsis*. The Journal of Biological Chemistry **277**, 20446–20452.

Liu P, Cheng Y, Yang M, Liu Y, Chen K, Long C, Deng X. 2014. Mechanisms of action for 2-phenylethanol isolated from *Kloeckera apiculata* in control of *Penicillium* molds of citrus fruits. BMC Microbiology **14**, 242.

Mateo-Bonmatí E, Casanova-Sáez R, Šimura J, Ljung K. 2021. Broadening the roles of UDP-glycosyltransferases in auxin homeostasis and plant development. New Phytologist **232**, 642–654.

Matsui D, Hirata Y, Iwakawa A, Toyotake Y, Wakayama M, Asano Y. 2021. Combination of enzymatic oxidation of amino acid and native chemical ligation with hydroxylamine for amide formation toward a one-pot process. Chemistry Letters **50**, 1632–1634.

McCoy AJ, Grosse-Kunstleve RW, Adams PD, Winn MD, Storoni LC, Read RJ. 2007. Phaser crystallographic software. Journal of Applied Crystallography **40**, 658–674.

Mellor N, Band LR, Pěnčík A, *et al*. 2016. Dynamic regulation of auxin oxidase and conjugating enzymes AtDAO1 and GH3 modulates auxin homeostasis. Proceedings of the National Academy of Sciences, USA **113**, 11022–11027.

Müller K, Dobrev PI, Pěnčík A, *et al*. 2021. DIOXYGENASE FOR AUXIN OXIDATION 1 catalyzes the oxidation of IAA amino acid conjugates. Plant Physiology **187**, 103–115.

Navarro-Llorens JM, Patrauchan MA, Stewart GR, Davies JE, Eltis LD, Mohn WW. 2005. Phenylacetate catabolism in *Rhodococcus* sp. strain RHA1: a central pathway for degradation of aromatic compounds. Journal of Bacteriology **187**, 4497–4504.

Pěnčík A, Casanova-Sáez R, Pilařová V, Žukauskaitė A, Pinto R, Micol JL, Ljung K, Novák O. 2018. Ultra-rapid auxin metabolite profiling for high-throughput mutant screening in Arabidopsis. Journal of Experimental Botany **69**, 2569–2579.

Pěnčík A, Rolčík J, Novák O, Magnus V, Barták P, Buchtík R, Salopek-Sondi B, Strnad M. 2009. Isolation of novel indole-3-acetic acid conjugates by immunoaffinity extraction. Talanta **80**, 651–655.

Perez VC, Dai R, Bai B, *et al*. 2021. Aldoximes are precursors of auxins in Arabidopsis and maize. New Phytologist **231**, 1449–1461.

Perez VC, Zhao H, Lin M, Kim J. 2023. Occurrence, function, and biosynthesis of the natural auxin phenylacetic acid (PAA) in plants. Plants **12**, 266.

Porco S, Pěnčík A, Rashed A, *et al*. 2016. Dioxygenase-encoding *AtDAO1* gene controls IAA oxidation and homeostasis in *Arabidopsis*. Proceedings of the National Academy of Sciences, USA **113**, 11016–11021.

Posit Team. 2023. RStudio: Integrated Development Environment for R. Boston, MA: Posit Software, PBC. http://www.posit.co/

Qin G, Gu H, Zhao Y, *et al*. 2005. An indole-3-acetic acid carboxyl methyltransferase regulates Arabidopsis leaf development. The Plant Cell **17**, 2693–2704.

Rampey RA, LeClere S, Kowalczyk M, Ljung K, Sandberg G, Bartel B. 2004. A family of auxin-conjugate hydrolases that contributes to free indole-3-acetic acid levels during Arabidopsis germination. Plant Physiology **135**, 978–988.

R Core Team. 2021. R: A language and environment for statistical computing. Vienna, Austria: R Foundation for Statistical Computing. https://www.R-project.org/

Schneider S, Mohamed ME-S, Fuchs G. 1997. Anaerobic metabolism of L-phenylalanine via benzoyl-CoA in the denitrifying bacterium *Thauera aromatica*. Archives of Microbiology **168**, 310–320.

Schwieter KE, Johnston JN. 2016. A one-pot amidation of primary nitroalkanes. Chemical Communications **52**, 152–155.

Sherp AM, Westfall CS, Alvarez S, Jez JM. 2018. *Arabidopsis thaliana* GH3.15 acyl acid amido synthetase has a highly specific substrate preference for the auxin precursor indole-3-butyric acid. The Journal of Biological Chemistry **293**, 4277–4288.

Široká J, Ament A, Mik V, *et al*. 2025. Amide conjugates of the jasmonate precursor *cis*-(+)-12-oxo-phytodienoic acid regulate its homeostasis during plant stress responses. Plant Physiology **197**, kiae636.

Staswick PE. 2009. The tryptophan conjugates of jasmonic and indole-3-acetic acids are endogenous auxin inhibitors. Plant Physiology **150**, 1310–1321.

Staswick PE, Rowe M, Spalding EP, Splitt BL. 2017. Jasmonoyl-L-tryptophan disrupts IAA activity through the AUX1 auxin permease. Frontiers in Plant Science **8**, 736.

Staswick PE, Serban B, Rowe M, Tiryaki I, Maldonado MT, Maldonado MC, Suza W. 2005. Characterization of an Arabidopsis enzyme family that conjugates amino acids to indole-3-acetic acid. The Plant Cell **17**, 616–627.

Stroganov OV, Novikov FN, Stroylov VS, Kulkov V, Chilov GG. 2008. Lead finder: an approach to improve accuracy of protein-ligand docking, binding energy estimation, and virtual screening. Journal of Chemical Information and Modeling **48**, 2371–2385.

Sugawara S, Mashiguchi K, Tanaka K, *et al*. 2015. Distinct characteristics of indole-3-acetic acid and phenylacetic acid, two common auxins in plants. Plant and Cell Physiology **56**, 1641–1654.

Takeuchi H, Fujimori Y, Ueda Y, Shibayama H, Nagaishi M, Yoshimura T, Sasamori T, Tokitoh N, Furuta T, Kawabata T. 2020. Solvent-dependent mechanism and stereochemistry of mitsunobu glycosylation with unprotected pyranoses. Organic Letters **22**, 4754–4759.

Takubo E, Kobayashi M, Hirai S, Aoi Y, Ge C, Dai X, Fukui K, Hayashi K-I, Zhao Y, Kasahara H. 2020. Role of Arabidopsis *INDOLE-3-ACETIC ACID CARBOXYL METHYLTRANSFERASE 1* in auxin metabolism. Biochemical and Biophysical Research Communications **527**, 1033–1038.

Tanaka K, Hayashi K, Natsume M, Kamiya Y, Sakakibara H, Kawaide H, Kasahara H. 2014. UGT74D1 catalyzes the glucosylation of 2-oxindole-3-acetic acid in the auxin metabolic pathway in *Arabidopsis*. Plant & Cell Physiology **55**, 218–228.

Teufel R, Mascaraque V, Ismail W, Voss M, Perera J, Eisenreich W, Haehnel W, Fuchs G. 2010. Bacterial phenylalanine and phenylacetate catabolic pathway revealed. Proceedings of the National Academy of Sciences, USA **107**, 14390–14395.

Thangavelu B, Mutthamsetty V, Wang Q, Viola RE. 2017. Design and optimization of aspartate *N*-acetyltransferase inhibitors for the potential treatment of Canavan disease. Bioorganic & Medicinal Chemistry **25**, 870–885.

Tickle IJ, Flensburg C, Keller P, Paciorek W, Sharff A, Vonrhein C, Bricogne G. 2016. STARANISO. Cambridge, UK: Global Phasing Ltd. http://staraniso.globalphasing.org/cgi-bin/staraniso.cgi

Tieman D, Taylor M, Schauer N, Fernie AR, Hanson AD, Klee HJ. 2006. Tomato aromatic amino acid decarboxylases participate in synthesis of the flavor volatiles 2-phenylethanol and 2-phenylacetaldehyde. Proceedings of the National Academy of Sciences, USA **103**, 8287–8292.

Tottman DR. 1987. The decimal code for the growth stages of cereals, with illustrations. Annals of Applied Biology **110**, 441–454.

Westfall CS, Sherp AM, Zubieta C, Alvarez S, Schraft E, Marcellin R, Ramirez L, Jez JM. 2016. Arabidopsis thaliana GH3.5 acyl acid amido synthetase mediates metabolic crosstalk in auxin and salicylic acid homeostasis. Proceedings of the National Academy of Sciences, USA **113**, 13917–13922.

Westfall CS, Zubieta C, Herrmann J, Kapp U, Nanao MH, Jez JM. 2012. Structural basis for prereceptor modulation of plant hormones by GH3 proteins. Science **336**, 1708–1711.

Wickham H. 2016. ggplot2: Elegant Graphics for Data Analysis. New York: Springer-Verlag.

Wickham H, Bryan J. 2023. readxl: Read Excel Files. R package version 1.4.3. https://CRAN.R-project.org/package=readxl.

Wickham H, François R, Henry L, Müller K, Vaughan D. 2023. dplyr: A grammar of data manipulation. R package version 1.1.4. https://CRAN.R-project.org/package=dplyr

Wightman F, Lighty DL. 1982. Identification of phenylacetic acid as a natural auxin in the shoots of higher plants. Physiologia Plantarum **55**, 17–24.

Xie Y, Zhu Y, Wang N, *et al*. 2022. Chemical genetic screening identifies nalacin as an inhibitor of GH3 amido synthetase for auxin conjugation. Proceedings of the National Academy of Sciences, USA **119**, e2209256119.

Xu S, Chen M, Feng T, Zhan L, Zhou L, Yu G. 2021. Use ggbreak to effectively utilize plotting space to deal with large datasets and outliers. Frontiers in Genetics **12**, 774846.

Yoo H, Widhalm JR, Qian Y, Maeda H, Cooper BR, Jannasch AS, Gonda I, Lewinsohn E, Rhodes D, Dudareva N. 2013. An alternative pathway contributes to phenylalanine biosynthesis in plants via a cytosolic tyrosine:phenylpyruvate aminotransferase. Nature Communications **4**, 2833.

Zasedateleva OA, Surzhikov SA, Shershov VE, Miftakhov RA, Yurasov DA, Kuznetsova VE, Chudinov AV. 2020. PCR incorporation of dUMPs modified with aromatic hydrocarbon substituents of different hydrophilicities: Synthesis of C5-modified dUTPs and PCR studies using Taq, Tth, Vent (exo-) and Deep Vent (exo-) polymerases. Bioorganic Chemistry **99**, 103829.

Zhang C, Zhang L, Wang D, Ma H, Liu B, Shi Z, Ma X, Chen Y, Chen Q. 2018. Evolutionary history of the glycoside hydrolase 3 (GH3) family based on the sequenced genomes of 48 plants and identification of jasmonic acid-related GH3 proteins in *Solanum tuberosum*. International Journal of Molecular Sciences **19**, 1850.

Zhang H, Cheng Q, Wang X, Jia W, Xie J, Fan G, Han C, Zhao X. 2022. Selenium improved phenylacetic acid content in oilseed rape and thus enhanced the prevention of *Sclerotinia sclerotiorum* by dimethachlon. Journal of Fungi **8**, 1193.